# Free-Volume Depth Profile of Polymeric Membranes Studied by Positron Annihilation Spectroscopy: Layer Structure from Interfacial Polymerization

**Hongmin Chen,[†] Wei-Song Hung,[‡] Chia-Hao Lo,[‡,§] Shu-Hsien Huang,[‡,§] Mei-Ling Cheng,[†,||] Guang Liu,[†] Kueir-Rarn Lee,[‡,§] Juin-Yih Lai,[‡,§] Yi-Ming Sun,[‡,||] Chien-Chieh Hu,[‡,#] R. Suzuki,[○] T. Ohdaira,[○] N. Oshima,[○] and Y. C. Jean*[,†,‡,§]**

*Department of Chemistry, University of Missouri—Kansas City, Kansas City, Missouri 64110, R&D Center for Membrane Technology, Chung Yuan Christian University, Chung-Li, 32023, Taiwan, Department of Chemical Engineering, Chung Yuan Christian University, Chung-Li, 32023, Taiwan, Department of Chemical Engineering and Materials Science, Yuan Ze University, Chung-Li, 32023, Taiwan, Department of Chemical Engineering, Nanya Institute of Technology, Chung-Li, 32023, Taiwan, and National Institute of Advanced Industrial Science and Technology, Ibaraki 305, Japan*

*Received July 6, 2007; Revised Manuscript Received August 8, 2007*

ABSTRACT: The free-volume depth profile of asymmetric polymeric membrane systems prepared by interfacial polymerization is studied using positron annihilation spectroscopy coupled with a variable monoenergy slow positron beam. Significant variations of *S*, *W*, and *R* parameters from the Doppler broadened energy spectra vs positron incident energy up to 30 keV and orthopositronium lifetime and intensity are observed at different doping times of triethylenetetraamine (TETA) reacting with trimesoyl chloride (TMC) in an interfacial polymerization on modified porous polyacrylonitrile (PAN) asymmetric membrane. The positron annihilation data are analyzed in terms of free-volume parameters as a function of depth from the surface to nano- and micrometer regions of asymmetric membranes. A multilayer structure is obtained in polymerized polyamide (PA) on modified PAN membranes (m-PAN): a nanometer scale skin polyamide layer, a nanometer to micrometer scale transition layer from dense to porous m-PAN, and the porous m-PAN support. The results of free-volume parameters and obtained layer thicknesses are compared with the flux (permeability) and water concentration in permeate (selectivity) through the pervaporation separation of 70 wt % 2-propanol aqueous solution. It is found that the water concentration in permeate is mainly controlled by the free-volume properties of skin polyamide and weakly related to the transition layer from the skin to porous m-PAN. The obtained layer structures of asymmetric polymeric membranes are supported by the data obtained by AFM, SEM, and ATR−FTIR.

## Introduction

A typical polymeric membrane system has a multilayered structure usually consisting of a thin surface layer, an intermediate layer, and a base substrate.[1] Each layer of the membrane system performs special functions and interacts with the other layers to achieve the main desired attributes of separation and filtration purposes.[2−5] For example, in the present day, a well-known asymmetric membrane for pervaporation process consists of a thin skin layer of polyamide (PA), which can be prepared by interfacial polymerization, a transition layer, and the supporting porous polymeric membrane.[6] The skin layer and also possibly the transition layer are thought to play a key role in the process of molecular diffusion and separation functions in pervaporation performance.[2,6]

While polymeric materials and layer systems have been used a long time for separation, purification, and storage, the basic understanding of physical structures and membrane interactions is still primitive.[1−6] There is limited understanding of the causes for performance in polymeric membrane systems, i.e., permeability and selectivity, at the molecular level.[7] Existing methods of assessing membrane performance are chiefly macroscopic approaches by a trial and error method, such as measuring macroscopic properties such as modulus, thermal stability, flow flux, and separation factors, etc.[1−7] Most knowledge of membrane development is based on these evaluations of performance[1−7] or by theoretical approaches.[8,9] Therefore, the origins of molecular transport phenomena are not yet fully ascertained for membrane systems. Only recently molecular spectroscopic and microscopic methodologies have been used to investigate the underlying causes of molecular transport phenomena in multilayer membrane systems.[10,11]

Analytical techniques which monitor the physicochemical parameters that occur during the preparation of membrane systems include spectroscopy methods, such as Fourier transform infrared (FTIR) and Raman spectroscopy,[10,12] where configurational and conformational variations are detectable. Resonance methods, such as nuclear magnetic resonance (NMR)[13,14] and electron spin resonance (ESR),[15,16] can detect local environments at the molecular level. Parameters in chemical properties are often correlated with changes in physical properties. Characterization of physical structures for a multilayer system of membranes has been pursued by scattering and microscopy methods, such as scanning electron microscopy (SEM),[17,18] transmitting electron microscopy (TEM),[19] atomic force microscopy (AFM),[20−22] X-ray,[23,24] electron, neutron, and ion diffractions, etc.[25−27] Each of these analytical techniques

[†] Department of Chemistry, University of Missouri—Kansas City.
[‡] R&D Center for Membrane Technology, Chung Yuan Christian University.
[§] Department of Chemical Engineering, Chung Yuan Christian University.
[||] Department of Chemical Engineering and Materials Science, Yuan Ze University.
[#] Department of Chemical Engineering, Nanya Institute of Technology.
[○] National Institute of Advanced Industrial Science and Technology.

10.1021/ma071493w CCC: $37.00 
Published on Web 09/22/2007

has its advantages and shortcomings in structural determination and elemental sensitivity. A multitechnique approach appears to be very fruitful. While X-ray diffraction and small-angle neutron scattering (SANS) are commonly used to measure defect and open space dimensions, they are limited to the larger dimensions (>nm). On the other hand, atomic probes, SEM, and AFM are powerful tools for detecting static defects near the surface. One important approach is to study the free-volume properties of polymeric membrane systems, the very origins of physical structure of polymers, i.e., from the Å to 1 nm level and $10^{-6} - 10^{-15}$ s time scale of motion[28,29]

The concept of correlating the physical defects at the atomic and molecular level, such as vacancy, free volume, holes, voids, interfaces, and surfaces, with membrane performances, such as permeability and selectivity, for optimal design of membranes is the central idea in this line of research. In this study, we employed a special physical technique, positron annihilation spectroscopy (PAS),[30] to measure physical properties of defects, i.e., free volumes at the atomic and molecular levels as a function of chemical changes and molecular modifications in an interfacial polymerized membrane system.

PAS[31] is a special nondestructive evaluation (NDE) technique for materials characterization which uses the positron (antielectron). Positron−electron annihilation $\gamma$-rays reveal useful information about the electronic and defect properties of materials under study. The unique repulsive force between the positron and the ion cores of materials makes the positron ideal for probing defects at the atomic and molecular levels. During the recent decades, PAS was developed as a useful tool to probe the microscopic properties of polymeric materials.[32] One of the great successes in this line of research is the direct determination of polymer free-volume and hole properties at an atomic scale (0.2−2 nm). However, most existing PAS studies focused on the bulk of polymers in measuring positron annihilation lifetime (PAL). Recent investigations in membrane systems using PAS have been reported and discussed mainly in the average bulk properties using the conventional PAL technique.[33−46]

Current positron spectroscopy uses a variable monoenergy positron beam (from the electronvolts range to several kiloelectronvolts)[47,48] coupled with PAL and momentum density measurements, and is capable of probing defect profiles from the surface, interfaces, and to the bulk. In this paper, we report a systematic investigation of both Doppler broadening energy spectroscopy (DBES) and PAL spectroscopy coupled with a variable monoenergy positron beam in one of the important membrane systems for pervaporation application, i.e., polyamide (PA) on modified asymmetric polyacrylonitrile (PAN) membrane.[6,49] In addition to the use of PAS technique, we recognize the importance of using conventional techniques to provide physical and chemical information including, ATR−FTIR, SEM, AFM, and pervaporation performances of flux (permeability) and water concentration in permeate (selectivity), to provide more complete information in the same membrane systems.

## Experiments

The currently studied polyamide membrane is a composite system with an asymmetric layer structure: a polyester nonwoven base substrate (ca. 150 $\mu$m thick), a porous supporting PAN (polyacrylonitrile, ca. 50 $\mu$m thick), and the top skin layer of interfacial polymerized polyamide (PA) as schematically shown in Figure 1. The porous support of PAN membrane was prepared by casting 15% PAN resin (supplied by Tong-Hua Synthetic Fiber Co. Ltd. Taiwan) in the solvent *N*-methyl-2-pyrrolidone (NMP) on the

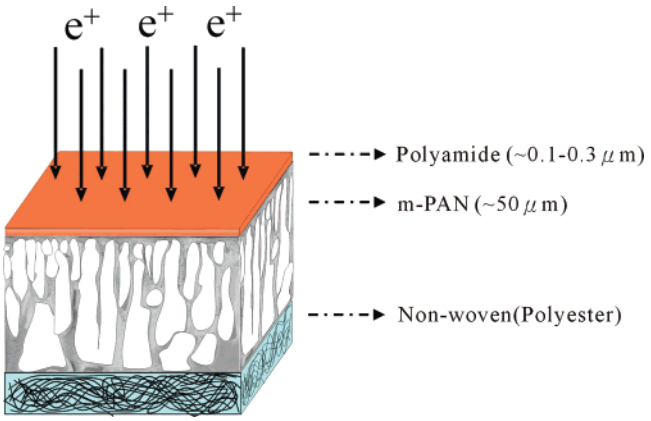


**Figure 1.** Schematic diagram for a multilayer asymmetric membrane system for the pervaporation and for positron annihilation studies. The top polyamide is synthesized from interfacial polymerization, the supporting membrane is polyacrylonitrile (ca. 50 $\mu$m), and the base substrate is nonwoven polyester (ca. 150 $\mu$m).

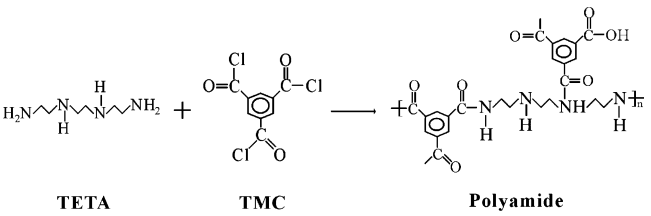


**Figure 2.** Schematic equation for interfacial polymerization reaction between triethylenetetraamine (TETA, aqueous phase) reacting with trimesoyl chloride (TMC, oil phase) to form polyamide (PA).

polyester nonwoven substrate with a 200 $\mu$m knife gap, then were immersed into water bath to precipitate. The resulting asymmetric PAN membranes (pore size 1−10 $\mu$m) were washed in water overnight and then were dried at ambient temperature. The asymmetric PAN membrane was posttreated in 2 M NaOH solution for 2 h at 50 °C. Fraction of the −CN groups of PAN supporting substrate can be converted into −COOH groups after the treatment of NaOH solution to enhance the interfacial polymerization reaction as monitored by ATR−FTIR. The average porosity of modified PAN was determined to be 82% from the density measurement. This modified (hydrolysis) asymmetric membrane is labeled as m-PAN.

The modified PAN porous membrane support (m-PAN) was washed in a water bath for several hours, and then dried at room temperature (rt). The polyamide active skin layer was synthesized using an interfacial polymerization technique on the m-PAN membrane support. A 2 wt % aqueous solution of TETA (triethylenetetraamine, purchased from Merck Co. USA) was doped onto the surface of the modified PAN support at 50 °C and as a function of doping times from 1 to 30 min, which are expected to vary membrane performance and structures. The m-PAN support soaked with the amine solution (aqueous phase) then was immersed into toluene solution (organic phase) containing 1 wt % TMC (trimesoyl chloride, purchased form Aldrich Chemical Co. USA) at rt for 3 min for interfacial polymerization. The excess amount of amine (TETA) solution remaining on the m-PAN membrane after interfacial polymerization was washed away and removed. The polymerization reaction and polyamide membrane preparation process are schematically shown in Figures 2and 3, respectively. The polyamide composite membrane systems were prepared at different TETA doping times (1−30 min) at 50 °C. The resulting membranes were washed in methanol overnight to remove any unreacted residual chemicals. After removal of toluene solution, the thin-film composite membranes obtained then underwent heat treatment in an oven at 70 °C for 1 h to attain the desired stability of the formed structure for characterization experiments. For the positron beam experiments, all samples were measured at the dry state under the high vacuum ($10^{-8}$ Torr). In the conventional PAL

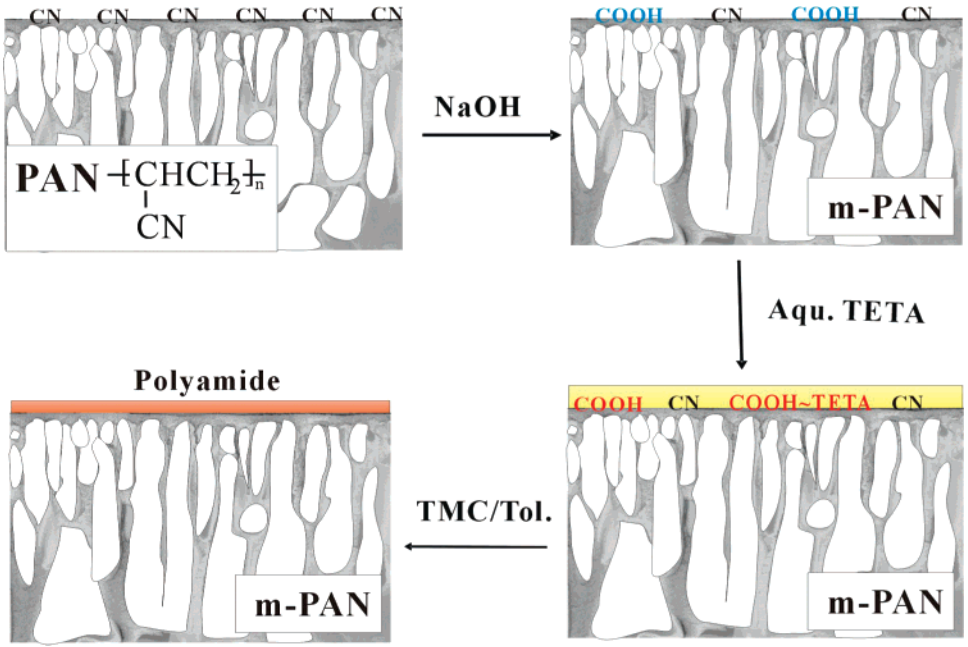


**Figure 3.** Preparation procedure of polyamide (PA) asymmetric membrane by interfacial polymerization between triethylenetetraamine (TETA, aqueous phase) reacting with trimesoyl chloride (TMC, oil phase) on modified PAN (polyacrylonitrile) surface, which is from hydrolysis of PAN membrane.

experiments, three wet samples were kept at the wet condition without changing water content in the process of PAL measurements (typically 3−4 h).

The layer thickness and surface morphology of the prepared PA on m-PAN and the m-PAN membrane were measured by AFM (Digital Instruments Nanoscope IIa tapping mode) and SEM (Hitachi model S-4800).

The performance of synthesized polyamide composite membranes was measured in the pervaporation of 70 wt % 2-propanol aqueous solution at rt. The feed solution is in direct contact with polyamide membrane and the flux is determined by the weight of permeate through pumping on the nonwoven side of the membrane. The composition of the feed solution and the concentration of permeate were determined using gas chromatography (GC Chromatography 8700 T, China). Detailed description of pervaporation measurements could be found in our previous work.[49]

The chemical structure of interfacial polymerized polyamide (PA) on the m-PAN supporting membrane is schematically shown in Figure 4. The functional groups of the prepared PA and m-PAN support are characterized by ATR−FTIR (Perkin-Elmer Spectrum One) at rt FTIR spectra of the m-PAN and one of interfacial polymerized PA (5 min doping TETA) on m-PAN as shown in Figure 5.

The *S* parameters of Doppler broadening energy spectra (DBES) were measured as a function of positron implantation energy (depth) at rt using the slow positron beam (0−30 keV) at the University of Missouri—Kansas City.[50,51] The DBES spectra were recorded at rt as a function of positron energy from 100 eV to 30 keV. The DBES spectra were measured using an HP Ge detector (EG&G Ortec. with 35% efficiency and energy resolution of 1.5 keV at 511 keV peak) at a counting rate of approximately 2500 cps. The total number of counts for each DBES spectrum was 2.0 millions. The obtained DBES spectra were characterized by an *S* parameter, defined as a ratio of integrated counts (area *A* of Figure 6) between energy 510.3 and 511.7 keV (*S* width) to total counts after the background was properly subtracted. Since the *S* parameter represents the relative value of the low momentum part of positron−electron annihilation radiation, it is sensitive to the change of the positron and positronium (Ps) states due to microstructural changes.[52−54] When the positron and Ps are localized in a hole or free volume with a finite size, the observed *S* parameter is a measure of the momentum broadening according to the uncertainty principle: a larger hole results in a larger *S* parameter value and the

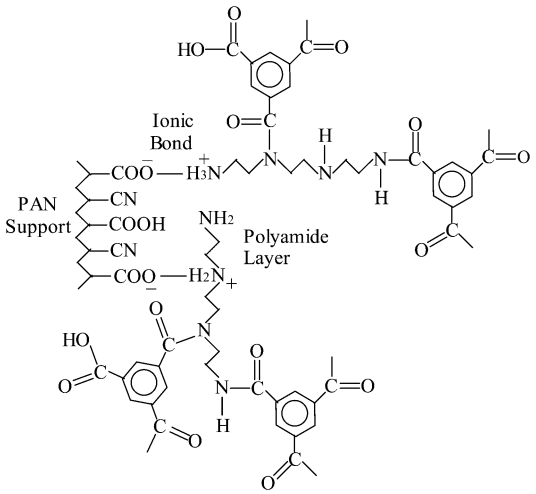


**Figure 4.** Schematic diagram of chemical structure for synthesized polyamide (PA) from interfacial polymerization between triethylenetetraamine (TETA, aqueous phase) reacting with trimesoyl chloride (TMC, oil phase) onto the surface of modified porous polyacrylonitrile (m-PAN membrane).

amount of parapositronium (singlet state). The *S* parameter has been successfully used in detecting the free-volume depth profile in polymeric systems.[52−54]

Two other parameters from DBES are also reported here: (1) the high momentum *W* parameter, which is defined as a ratio of integrated counts (area *B* of Figure 6) between energy 508.0 and 509.4 keV (left *W* width) and energy 512.6 and 514.0 keV (right *W* width) to total counts after the background was properly subtracted, and (2) the $3\gamma$ to $2\gamma$ annihilation ratio *R* parameter, which is defined as the ratio of the total count from the valley region with an energy with a width between 364.2 and 496.2 keV (which is from $3\gamma$ annihilation) and the total count from the 511 keV peak region with a width between $E_1 = 504.35$ and $E_2 = 517.65$ keV (which is from $2\gamma$ annihilation). The *R* parameter provides information about the existence of large pores (nm to $\mu$m), where o-Ps undergoes $3\gamma$ annihilation while *S*, and *W* are from p-Ps and o-Ps undergoing $2\gamma$ radiation (pick-off annihilation) in free volumes (Å to nm). The definitions of *S*, *W*, and *R* from DBES

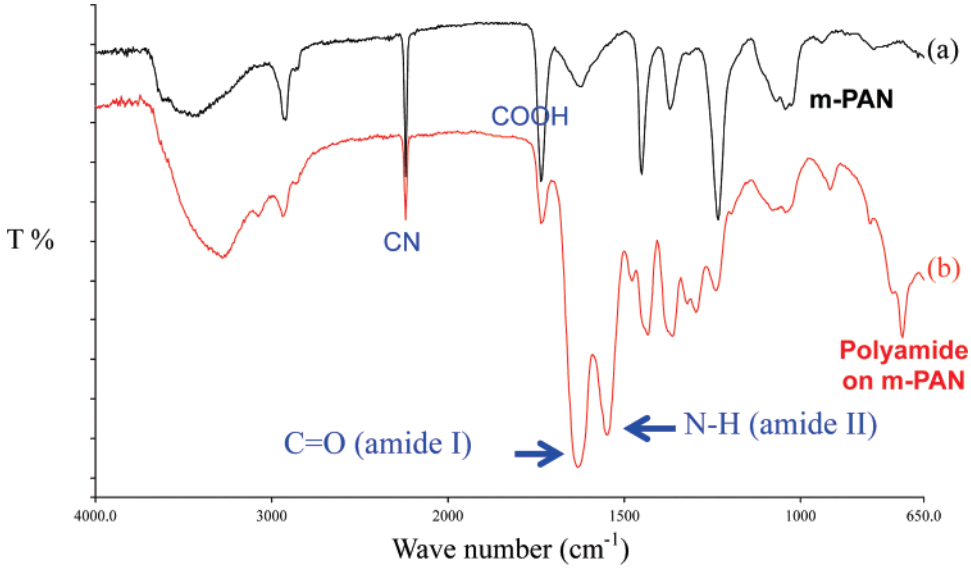


**Figure 5.** ATR−FTIR spectra for modified polyacrylonitrile (m-PAN) membrane and for polyamide (PA) from interfacial polymerization between triethylenetetraamine (TETA) reacting with trimesoyl chloride (TMC) on m-PAN.

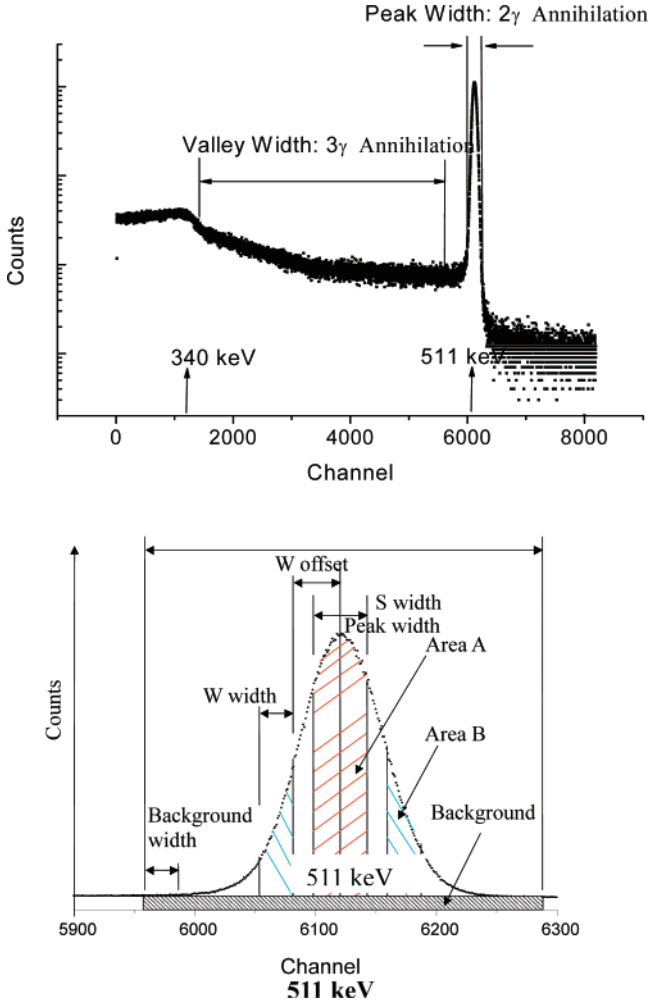


**Figure 6.** Doppler broadening energy spectrum (DBES, top) and definitions of *S*, *W*, and *R* ($3\gamma/2\gamma$ ratio) parameters from DBES. *S* is ratio of total counts from central region, *W* is the ratio of wing region, to the total 511 keV annihilation counts, respectively, while *R* is the ratio of $3\gamma/2\gamma$ annihilation.

are schematically shown in Figure 6. The detailed description of the beam and *S*, *W*, and *R* parameter measurements could be found elsewhere.[30,47,48]

Positron annihilation lifetime experiments were performed using both a variable monoenergy 30 keV positron beam at UMKC[50,51] and a high intense slow positron beam at the National Institute of Advanced Industrial Science and Technology (AIST) in Tsukuba, Japan.[55] We also used the conventional PAL method[32] to measure the free-volume properties in the bulk (thick film ∼1 mm) membrane samples. The PAL data contain quantitative information on the free-volume properties in polymeric systems from the surface, interfaces, and to the bulk. The lifetime resolution was 450−800 ps and 250−500 ps for a counting rate of 100−500 cps and 1000−2500 cps at UMKC's and at AIST's slow positron beam, respectively. Each PAL spectrum contains 2 million counts. The obtained PAL data were fitted into four lifetime components using the PATFIT program[56] and also into continuous lifetime distributions using three existing programs: CONTIN,[57] LT,[58] and MELT.[59] While the latter three programs provide similar results, we only present the smoothed lifetime distributions from MELT analysis here. In PATFIT analysis, the longest lifetime component (8−40 ns) from the beam experiments at a small intensity 0.3−5% (10−0.3 keV positron energies) was attributed to o-Ps annihilation in the beam chamber from backscattered positrons and surfaces. PAL spectra in an interfacial polymerized polyamide (5 min TETA doping time) on m-PAN membrane at different positron energies (depths) are shown in Figure 7. It is seen that both o-Ps lifetime and intensity vary as a function of incident positron energy due to different layer structure, chemical composition, and polymeric properties at different depths from the surface.

Analyzed results of positron lifetimes ($\tau_1$, $\tau_2$, and $\tau_3$) and intensities ($I_1$, $I_2$, and $I_3$) from PAL spectra are attributed to the positron and positronium annihilation in polymeric membrane materials. The shortest $\tau_1 = 0.125$ ns (constrained in our final PATFIT analysis) is from p-Ps annihilation, $\tau_2 \sim 0.45$ ns is from the positron annihilation, and $\tau_3$ is due to o-Ps annihilation. Since Ps is known to preferentially localize in defect sites,[60] particularly in the free volume before annihilation takes place, parameters from o-Ps annihilation have been successfully used to obtain the electron properties and depth profiles of free volumes in thin film polymers.[61−64] The o-Ps lifetime $\tau_3$ is on the order of 1−5 ns in polymeric materials, the so-called pickoff annihilation with electrons in molecules[32] and is used to calculate the mean free-volume radiusR (Å to nm) based on an established semiempirical correlation equation[65−67] from a spherical-cavity model.

When a positron enters the polymeric surface, it loses its energy via inelastic collision processes within the time scale of $10^{-12}$ s, and its energy distribution could be expressed by a Makhovian implantation profile. The mean depth *Z* of the polymeric materials

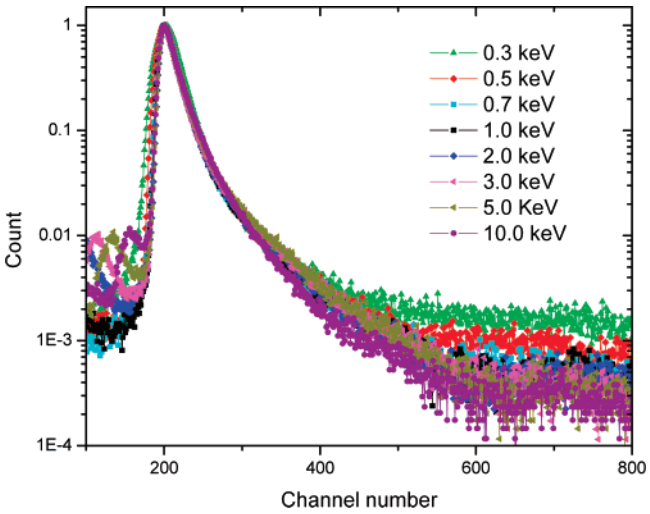


**Figure 7.** 7. Normalized positron annihilation lifetime (PAL) spectra at different positron incident energies in an interfacial polymerized polyamide (with 5 min of TETA doping time) on m-PAN. One channel corresponds to 25 ps.

where the positron annihilation occurs is calculated from $E_+$ using eq 1 below:[47,48]

$$Z(E_+) = (40/\rho)E_+^{1.6} \quad (1)$$

where $Z$ is expressed in nm, $\rho$ is the density in g/cm$^3$, and $E_+$ is the positron incident energy in keV. The corresponding distribution of the depth $Z$ is broadened with the increase of positron energy $E_+$ and the depth resolution is better near the surface than in the bulk. A typical depth resolution is estimated to be about 10% of the depth of interest.

## Results and Discussion

**I. Modified PAN Membrane and Polyamide.** In order to study the interfacial polymerized polyamide (PA) membrane system, we have performed the DBES data in PA and modified (hydrolysis) PAN (m-PAN) membranes as a function of positron incident energy (0−30 keV) at rt At the same time, we also performed PAL experiments in the base materials, PAN membrane, m-PAN membrane, and polyamide (PA) resin in both dry and wet (after soaking in 70% 2-propanol aqueous solution for 24 h) states. The base materials of PAN and m-PAN were prepared in similar method as membranes except on the glass substrate instead of nonwoven polyester base substrate. We peeled off the prepared membranes, packed the samples (porosity 82%) at a thickness of >1 mm, which is sufficient to absorb all positrons emitted from $^{22}$Na source. Table 1 lists the analyzed PAL results of those six materials in the currently studied membrane system. For porous membranes PAN and m-PAN, which contain high porosity (82%) with a pores size on the order of $\mu$m, we observed additional small fraction of very long o-Ps lifetime (120−140 ns) with intensity of 1.0, and 1.5 ± 0.4%, respectively from long gated PAL spectra (500 ns). The very long o-Ps lifetime is contributed from those large pores ($\mu$m) and their lifetime is beyond the sensitivity of current PAL to distinguish their sizes. Our focus is on the third component, i.e., $\tau_3$ and $I_3$, to calculate the free-volume hole properties according to the established correlations from the pick-off annihilation.[32,65−67]

It is seen in Table 1 that the o-Ps lifetime ($\tau_3$) from of those six polymeric materials are in the values of similar polymers[33−45,68−70] as o-Ps pick-off annihilation and the corresponding free-volume radius ranges from 0.25 to 0.40 nm. It is interesting to observe that polyamide has a smaller free volume than both PAN and m-PAN. To understand the free-volume size distributions in those polymers, we have analyzed the positron lifetime distributions and the $\tau_3$ results (with corresponding free-volume radius distributions) are shown in Figure 8 for both dry and wet samples. The shapes of o-Ps lifetime distributions are similar while both the lifetime values and widths of the distributions are in the order of PAN > m-PAN > PA. In the same graph, we also show the kinetic radii of water[71] and 2-propanol[72] to compare with the free-volume radius distributions in those base polymers obtained by PAS. It is interesting to observe that PA radius lies apart from and between the kinetic radius of water (1.3 Å) and of 2-propanol (2.9 Å). On the other hand, the free-volume radius distributions of both PAN and m-PAN are all larger than both water and 2-propanol. The selectivity for permeatants in polymeric membranes has been traditionally understood in terms of molecular interactions with polymers. The current PAS studies could provide a new approach in terms of size selectivity of free volume for permeatants to explain the effective selectivity of polyamide used in pervaporation applications (water concentration in permeate >95%) for water/2-propanol separation and the low water concentration in permeate observed in m-PAN membranes without PA (<50%). For diffusivity, we expect that pervaporation performance, i.e., water concentration in permeate, for membrane with an interfacial polymerized PA layer may be correlated with the free-volume data. In Table 1, we also report the o-Ps results in the wet states of membrane and PA polymers in which pervaporation measurements were performed. We found that the wet m-PAN has a larger $\tau_3$ (3.295 ± 0.018 ns) than the dry membrane (2.572 ± 0.031 ns). On the other hand, we found that the soaking in 2-propanol aqueous solution for 24 h has very little effect on the o-Ps lifetime in the bulk polyamide ($\tau_3$ = 2.081 ± 0.021 ns, = 2.099 ± 0.015 ns for dry, and wet PA, respectively). The observed large $\tau_3$ in wet m-PAN may be due to the contribution of the soaked 70% 2-propanol aqueous solution, which has a large $\tau_3$ (=3.552 ± 0.021 ns, with $I_3$ = 16.44 ± 0.15%) and also possibly the swelling of free-volume in wet m-PAN by the interaction between 2-propanol or water with the m-PAN. We further dried the wet m-PAN membrane sample and then measured PAL again. We found that the PAL result ($\tau_3$ and $I_3$) returns to the values as listed in Table 1 of the original dry m-PAN sample. This shows that the m-PAN membrane retains its chemical compositions and layer structures after pervaporation applications.

We also performed the AFM and SEM on both m-PAN and polymerized PA/m-PAN membranes to measure the surface morphology and the cross sections. Figures 9−11show the surface images and cross sections from AFM and SEM experiments. From AFM data (part b of Figure 9), we observe that the mean-squares surface roughness ($R_{ms}$) in m-PAN is relatively small, 24.8 nm, which could be due to the reaction of NaOH with PAN. On the other hand, the roughness in polymerized PA/m-PAN surfaces is relatively large. For example, in the PA surface with 5 min of TETA doping (part d of Figure 9), $R_{ms}$ is 87.2 nm. The results of surface roughness from AFM are listed in Table 2. It has been reported that the flux of pervaporation in the similar membrane systems increases as the surface roughness increases due to the increase of skin surface area.[73] The relative roughness and skin layer thicknesses will be compared with PA interfacial polymerized membrane and discussed in the next section.

The SEM cross section images of PA and m-PAN are rather interesting as shown in Figures 10 and 11. In the m-PAN

**Table 1. Positron Lifetime Results in Base Materials for Membrane Systems[a]**

| sample | $\tau_2$ (ns) | $I_2$ (%) | $I_3$ (%) | $\tau_3$ (ns) | $R$ (Å) | FFV (%) |
|---|---|---|---|---|---|---|
| polyamide (PA)−dry | 0.417 ± 0.012 | 62.2 ± 0.5 | 7.73 ± 0.2 | 2.081 ± 0.021 | 2.92 ± 0.07 | 1.45 ± 0.29 |
| m−PAN membrane−dry | 0.469 ± 0.032 | 53.6 ± 0.3 | 9.33 ± 0.2 | 2.268 ± 0.018 | 3.08 ± 0.03 | 2.06 ± 0.21 |
| PAN membrane−dry | 0.465 ± 0.035 | 58.9 ± 0.3 | 6.82 ± 0.2 | 2.572 ± 0.031 | 3.32 ± 0.04 | 1.89 ± 0.21 |
| polyamide (PA)−wet | 0.468 ± 0.010 | 57.9 ± 0.5 | 7.86 ± 0.2 | 2.099 ± 0.021 | 2.99 ± 0.07 | 1.50 ± 0.29 |
| m−PAN membrane−wet | 0.460 ± 0.021 | 66.6 ± 0.3 | 12.88 ± 0.2 | 3.295 ± 0.018 | 3.82 ± 0.03 | 5.42 ± 0.21 |
| PAN membrane−wet | 0.480 ± 0.030 | 60.9 ± 0.3 | 12.03 ± 0.2 | 3.449 ± 0.023 | 3.92 ± 0.04 | 5.45 ± 0.21 |

[a] Notes: (1) The shortest lifetime time $\tau_1$ was fixed to 0.125 ns in PATFIT analysis. (2) m-PAN membrane is the modified (hydrolysis) PAN membrane for PAN membrane reacts with 2 M of NaOH solution. (3) Wet samples were soaked the same dry samples in 70% 2-propanol aqueous solution. (4) R, and FFV are the mean free-volume radius, and the relative free-volume fractions, respectively estimated from o-Ps data according to semiempirical equations.[32,65−67]

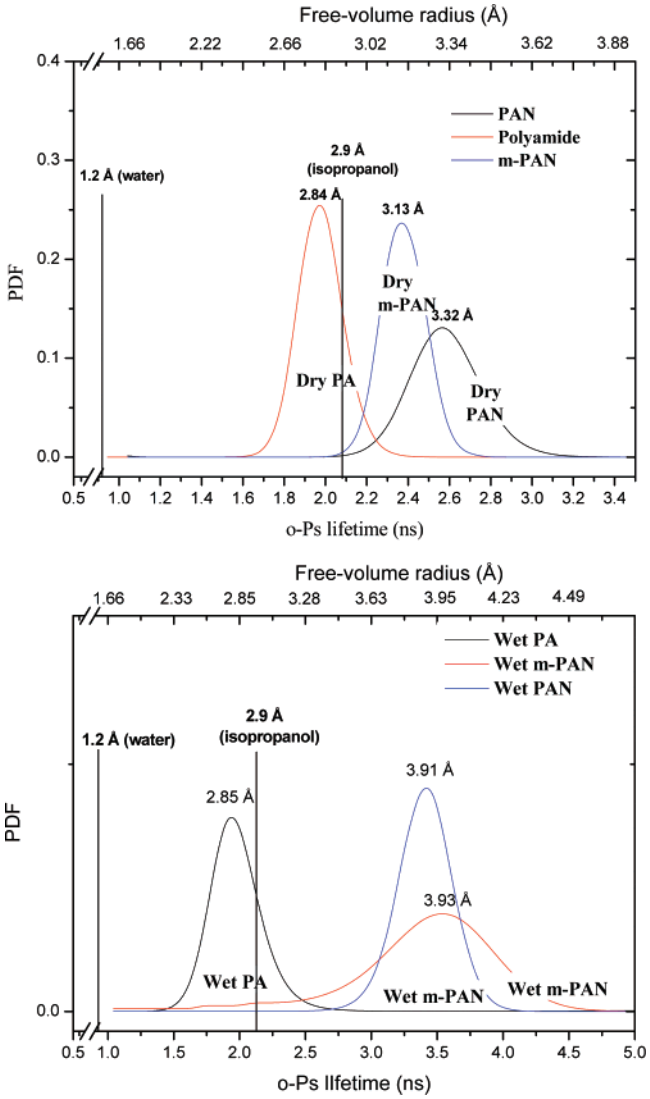


**Figure 8.** Mean free-volume radius and o-Ps lifetime distributions in dry (top plots) and wet states (bottom plots) of bulk polyamide (PA), porous PAN, m-PAN porous membranes. Kinetic radii of water and 2-propanol were taken from refs 71 and 72, and the numbers in each distribution are the mean radii obtained from the mean lifetimes of MELT[59] analysis.

membrane, we observe a skin layer on top of porous m-PAN membrane as indicated in Figure 10 (top). The thickness of this skin surface layer in m-PAN is found to be 402 ± 70 nm (from an average of five measurements). From the contrast of the images, this skin layer shows a density greater than the porous layer beneath it. Its density is found to be close to the density of the bulk m-PAN as to be confirmed from positron data next that this layer has a density as the bulk value of m-PAN, i.e., $\rho = 1.2$ g/cm$^3$. From the SEM data, we also observe the pore size of m-PAN inside the dense skin layer is between 1 and 10 $\mu$m. From SEM cross sections near the surface, we also see that there is certain intermediate depth (nano- to micrometer) between the dense skin layer and the porous m-PAN layer (50 $\mu$m). We call this intermediate depth a transition layer from the dense skin of m-PAN to the porous m-PAN. From SEM images, we estimated the thickness of this transition layer in m-PAN to be on the order of 1 $\mu$m. We also see the inner layer with a high porosity in the SEM cross-section image (Figures 10 and 11). SEM images of m-PAN are compared with the PA/m-PAN membranes in Figure 11. The indicated skin thickness from SEM cross section in PA/m-PAN membrane shown in Figures 10 and 11 are the synthesized PA layer on top of the dense skin of m-PAN. For example, in a 5-min TETA doping membrane, the PA thickness was determined to be 326 ± 10 nm as indicated in Figure 10 (bottom) and Figure 11. The layer thickness from SEM for different TETA doping times will be discussed in the next section along with the positron data.

We have performed DBES experiments as a function of the depth in two base membrane materials, the m-PAN membrane and the polyamide resin. The data of $S$ vs positron incident energy (or depth) are shown in Figure 12 (top). From those $S$ data we have the following observations: (1) $S$ near the surface increases sharply as the positron energy increases; (2) $S$ reaches a maximum and then decreases for m-PAN before plateau, while for PA there is no peak; and (3) $S$ values for m-PAN are all larger than those for PA.

First, the third observation on the trend of $S$ values m-PAN > PA could be understood from the origin of $S$, which is mainly due to the para-Ps (singlet positronium) contribution of positron annihilation near the annihilation energy 511 keV.[52−54] This trend is also seen in the o-Ps parameters obtained by the positron annihilation lifetime experiments (Table 1).

Next, the sharp increase of $S$ near the surface is a typical phenomenon for polymeric materials due to annihilation of positronium, which is known to have a very short diffusion length in polymeric materials, on the order of 1−20 nm.[60,74] A peak in $S$ vs depth variation is an indication of a multilayer structure in the system from annihilation characteristic difference between those layers. We have employed a computer program VEPFIT,[75] which takes the Makhovian distribution of positron energy into consideration and also includes the surface annihilation and epithermal positron/Ps diffusion into its fitting algorithm. We have tried to fit two-, three-, and four-layer models in the VEPFIT analysis. The two-layer model could not give good enough $\chi^2$ values, which are all consistently greater than 10.0 for m-PAN and thus do not give an acceptable model for m-PAN data. While the four-layer model gives slightly better $\chi^2$ values than the three-layer model, the fitted results are unstable and the resultant error bars are larger than the fitted layer and diffusion lengths. We found that the results from three-layer model fits have good $\chi^2$ values (<2.5) and give stable

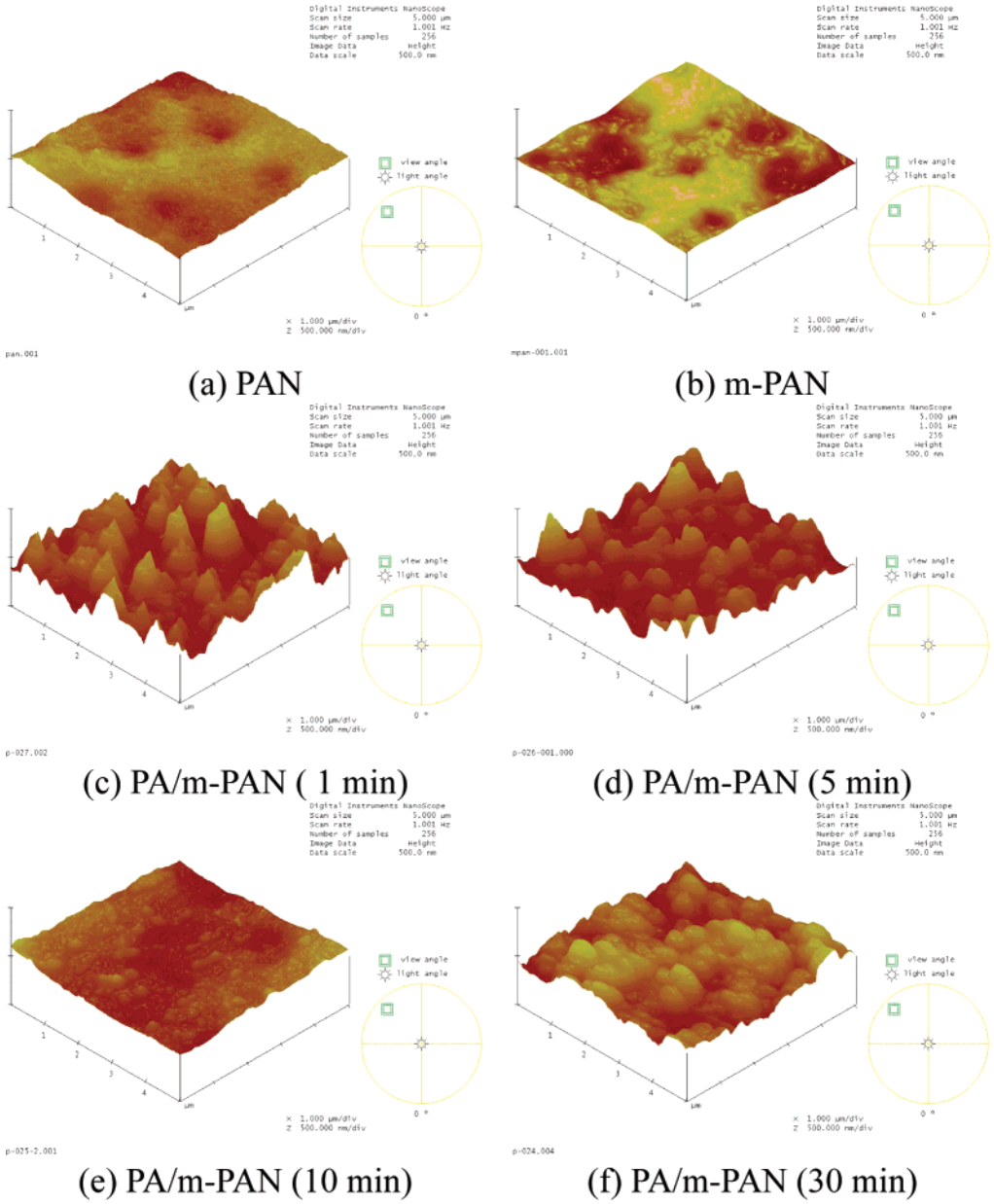


**Figure 9.** AFM images of the PAN, modified PAN (m-PAN) and polyamide (PA) on the m-PAN asymmetric membrane. Key: (a) PAN membrane, (b) m-PAN membrane, (c) PA/m-PAN with 1 min TETA doping time, (d) PA/m-PAN with 5 min TETA doping time, (e) PA/m-PAN with 10 min TETA doping time, and (f) PA/m-PAN with 30 min TETA doping time.

results and reasonable error bars. Therefore, we report here the results of three-layer fits in Table 3 for m-PAN membrane and discuss the layer structures based on three-layer model results. On the other hand, for *S* data in PA, the two-layer model gives good and reasonable results. Fitted lines from VEPFIT analysis are also plotted in Figure 12, which shows the good fits of the three-layer model for m-PAN membrane and the two-layer model for PA resin, respectively.

The top layer for m-PAN (with a thickness of 200 ± 117 nm) is identified as the dense skin layer as we also found that the best fit density of this layer is 1.2 ± 0.1 g/cm$^3$, which is the same value as the bulk m-PAN resin. Its positron/Ps diffusion length, 61.7 ± 16.7 nm, is slightly longer than most neat polymers (1−20 nm),[60,74] indicating that the skin may be denser than bulk m-PAN resin. The reason for the best fit density 1.2 ± 0.1 g/cm$^3$ may be due to a combination of surface roughness (with some open space and less dense) and the dense skin (with a density possibly greater than 1.2 ± 0.1 g/cm$^3$). The length of the intermediate (transition) layer is found to be much larger, 2.6 ± 1.6 $\mu$m with a density of 1.0 ± 0.1 g/cm$^3$, which is in between the bulk m-PAN (1.2 ± 0.1 g/cm$^3$) and the porous m-PAN beneath it. The third layer is identified as the porous m-PAN, which has a fitted density of 0.7 ± 0.1 g/cm$^3$, which is still larger than the 0.22 g/cm$^3$ as measured in the porous m-PAN (82% average porosity). This indicates that the structure of m-PAN between 2 and 10 $\mu$m is still not as porous as the average porosity of the entire m-PAN membrane. The fitted *S* parameters for the second layer and the third layer are close to each other and it indicates that there is a progressive transition in the porosity from the second layer to the third layer in the m-PAN membrane.

This layer analysis from *S* data is further supported by the *R* data vs the depth as shown in Figure 12 (bottom plot) since *R* is a measure of relative amount of 3 $\gamma$ annihilation which could be contributed only from o-Ps in vacuum or in large pores. As shown in the *R* plot, we observe large values near the surface and also inside the m-PAN membrane. For PA, since there are no large pores inside the polymer, we observe a flat value of *R*

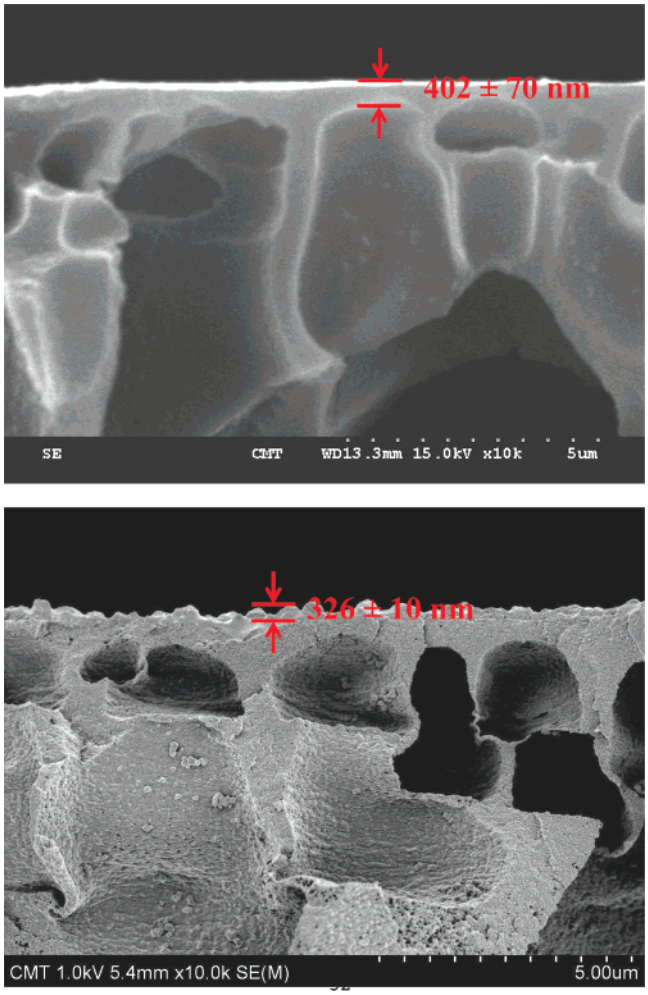


**Figure 10.** SEM cross section images of the m-PAN (top) and polymerized PA (with 5 min TETA doping) on m-PAN membrane. The indicated thickness in m-PAN (top) is for the dense skin m-PAN while the thickness for the bottom image is for the PA skin layer (with 5 min TETA doping) from interfacial polymerization on top of dense skin of m-PAN and porous m-PAN. The magnification is ×10 000 and the pore size for m-PAN is between 1 and 10 $\mu$m.

at the depth inside the surface (a few nanometers). In the m-PAN, we observe a slow increase of $R$ from about 200 nm and then largely increase at about 500 nm from the surface. This is due to the contribution of o-Ps from the pore starting 500 nm beyond the dense skin layer of m-PAN. The increasing $R$ parameter between 0.5 and 2.0 $\mu$m is identified as a transition layer between the dense skin and porous m-PAN membrane. The plateau of $R$ from the depth greater than 3−4 $\mu$m in Figure 12 (bottom plot) shows the contribution from large pores ($\mu$m) due to 3 $\gamma$ annihilation of o-Ps.

From the results of $S$ vs depth analysis, the $R$ vs depth, and with the aid of SEM images, we obtain the layer structure for the m-PAN membrane as schematically shown in Figure 13. It is worthwhile to note that while the skin layer thickness from PAS and SEM images show a consistent result in the membrane layer structures, $S$ data provides additional information about the gradient of porosity or density as a function of the depth and also is able to resolve a transition layer between the skin and porous layers. This observed transition layer on the order of a few micrometers, which has not been observed previously by other techniques, has been used in the theoretical models for mass transport phenomena.[8,9]

**II. Interfacial Polymerized Polyamide/m-PAN Membranes.** Interfacial polymerization occurs when TETA in the aqueous phase reacts with TMC in the oil phase and then produces a skin polyamide layer on top of the m-PAN membrane. The layer structure of the interfacial polymerized PA membrane varies as a function of experimental parameters, such as time of doping in aqueous phase, temperature of doping, chemical structures of amines and organic chlorides and their weight percent.[6,49] In this study, we chose the experimental parameter as the period of doping time of TETA in m-PAN membranes at 50 °C. We measured the DBES as a function of positron energy to 30 keV in the interfacial polymerized membranes prepared with four different periods of TETA doping time (1, 5, 10, and 30 min). Figure 14 shows the obtained $S$ parameter vs the positron incident energy or the mean depth by using an established eq 1 for four doping times at 50 °C. We have the following observations: (1) $S$ value is small near the surface and then increases as the depth increases. (2) There is a kink, i.e., nearly flat value of $S$ vs the depth some distance from the surface of the membranes, i.e., < 0.2 $\mu$m and the location of the kink shifts to the surface as a function of TETA doping time. (3) $S$ increases to a maximum as the depth increases and the peak $S$ value increases with the doping time. (4) After the peak, $S$ slightly decreases as a function of depth and eventually all $S$ at different doping times converge at a depth about 2 $\mu$m.

To understand the variations of $S$ vs depth, we follow the same procedure above similar to the m-PAN membrane by using the VEPFIT analysis.[75] Although the $S$-depth variations (Figure 14) for PA/m-PAN membranes are seen to be different from those from the m-PAN membrane (Figure 12), particularly additional kinks (nearly flat S) near the surface, we found that the best fitted results as judged from good $\chi^2$ values ($\chi^2 < 2.5$) and reasonable error bars are also from the three-layer model fits. On the basis of the same justifications that in four-layer fits, error bars of layer and diffusion lengths are larger than the lengths, we adopt the three-layer results for the following discussions. The resulting $S$, positron diffusion lengths, layer thicknesses, and densities from three-layer fits are listed in Table 4, and the fitted lines are also shown in Figure 14.

To interpret the $S$ variation in terms of layer structure in interfacial polymerized membrane systems, we should consider their chemical compositions along with the physical structures of each layer. There are two possible types of chemical compositions from the surface to 10 $\mu$m, i.e., polyamide (PA) and m-PAN. First, since we know that the $S$ values have an order of m-PAN > PA in the above section (Figure 12), it is reasonable to assume the kink of $S$ near the surface is due to the presence of interfacial polymerized PA. The contribution of PA is expected to decrease as the depth increases into the inner layers.

Next for the second layer, we proceed with the interpretation similar to that discussed in the m-PAN membrane. We assign the intermediate layer as a transition layer from the dense skin to the porous m-PAN since the peak values of $S$ near 0.3−0.7 $\mu$m (Figure 14) are approaching the same peak value (0.48) of the m-PAN (Figure 12). A shift of the peak position to the depth in PA/m-PAN over the m-PAN is due to the presence of additional thickness from PA on PA/m-PAN membrane. Furthermore, for the third (inside the peak) layer, we assign it as a layer as the porous m-PAN membrane. This assignment of layer 1, 2, and 3 as skin PA, dense to porous m-PAN, and porous m-PAN, respectively, could be confirmed from three ways: (1) The plots of $S$ (peak parameter) vs $W$ (wing parameter) and $R$ ($3\gamma/2\gamma$ ratio) from DBES; (2) the PAL data as a function of the depth; and (3) by the aid of the SEM and AFM images.

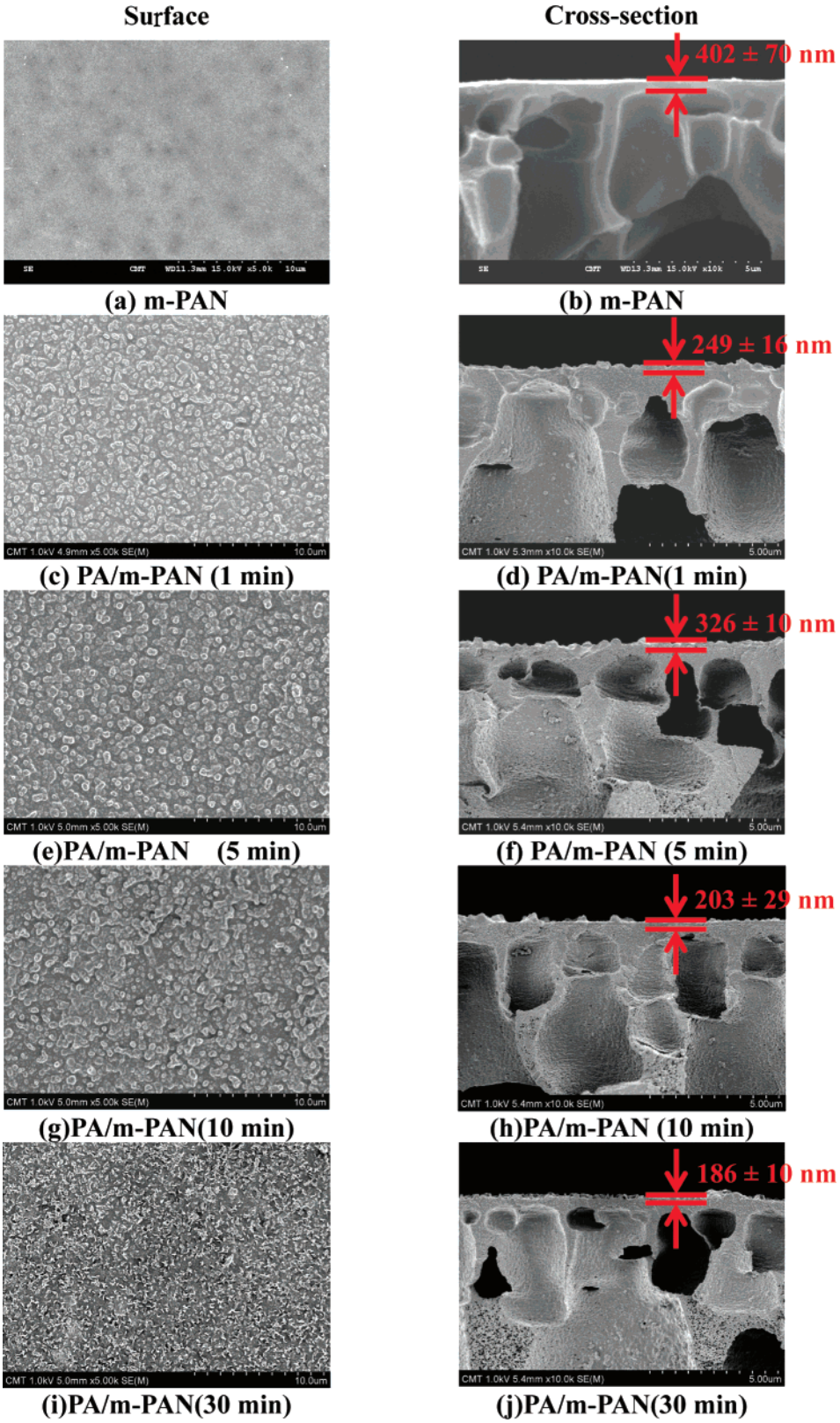


**Figure 11.** SEM images of m-PAN and polymerized PA (1−30 min of TETA doping time) on m-PAN membrane. The magnification is ×10 000. The indicated thickness of top layer for m-PAN (b) is the dense m-PAN skin while those for polymerized PA on m-PAN (d, f, h, and j) are the PA layer on top of the dense m-PAN.

Figure 15 shows two *S* vs *W* plots from the five sets of DBES data, i.e., 0 (unreacted), 1, 5, 10, and 30 min of TETA doping times. In DBES, *W* is a parameter from the wing regions of 511 keV annihilation radiation (Figure 6) and it is an indication of types of chemical elements or defect types in DBES data.[31,47,48] As shown in Figure 15 from S/W plots, we could identify two regions of data, which show two slopes, one group near left top region (large *W*/small *S*) and the other at the right bottom region (small *W*/large *S*). Two lines fitted into these two regions are shown in Figure 15 for both m-PAN and PA/m-PAN membranes. The intercepts coincide with the locations where we observe the largest transitions of *S* vs depth (Figures

**Table 2. Surface Roughness Values of PAN, m-PAN and Polyamide (PA)/m-PAN Asymmetric Membranes[a]**

| membranes | $R_{ms}$ (nm) | $R_a$ (nm) | $R_{max}$ (nm) |
|---|---|---|---|
| PAN | 28.5 | 24.0 | 180.7 |
| m−PAN | 24.8 | 20.4 | 119.1 |
| PA/m−PAN (1 min) | 99.4 | 80.9 | 617.8 |
| PA/m−PAN (5 min) | 87.2 | 67.8 | 603.1 |
| PA/m−PAN (10 min) | 29.6 | 24.6 | 195.9 |
| PA/m−PAN (30 min) | 64.9 | 52.5 | 383.4 |

[a] Note: $R_{ms}$, $R_a$, and $R_{max}$ are mean-squares, average, and maximum roughness, respectively, from AFM images.

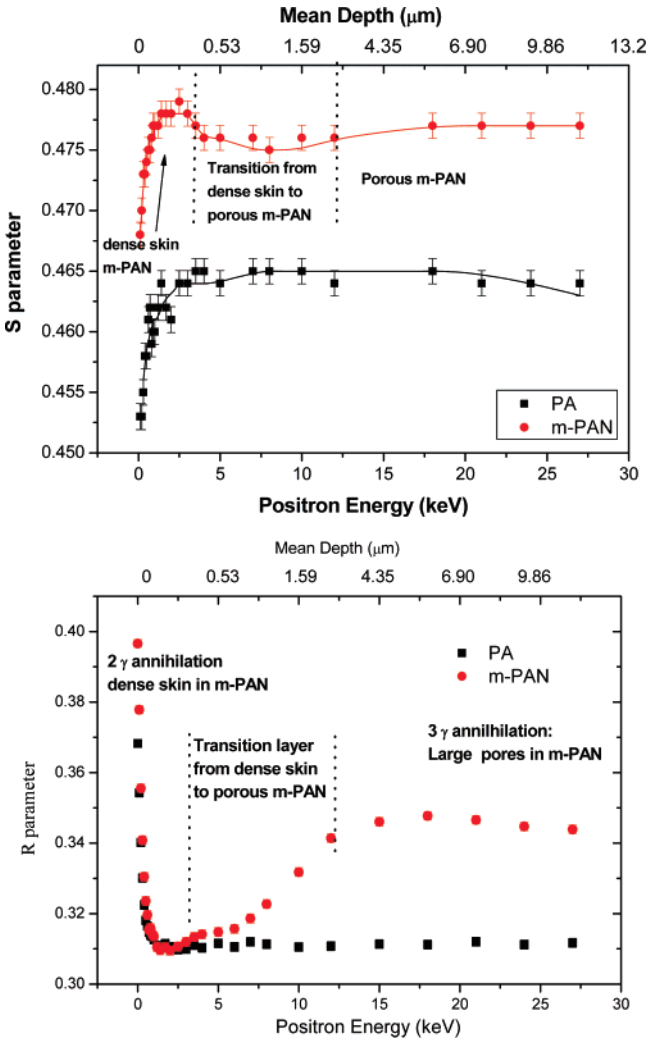


**Figure 12.** *S* (top) and *R* (bottom) parameters vs positron incident energy (or depth) in PA resin and m-PAN membrane. The lines for *S* parameters are fitted results from VEPFIT[75] analysis in three-layer and two-layer model for m-PAN, and for PA, respectively. Vertical dot lines indicate the boundaries from layer to layer in m-PAN.

12 and 14) i.e. at the boundary of layers one and two. A break in the *S*/*W* plot (top plot of Figure 15) for m-PAN indicates a transition from the dense skin structure to the porous m-PAN membrane. For PA/m-PAN (bottom plot of Figure 15), a different slope indicates a chemical composition transition in the depth profile, which is a transition from PA to m-PAN.

Next, Figure 16 shows a plot of *R* parameter ($3\gamma/2\gamma$ ratio) vs the positron energy (depth) from the four sets of DBES data in 1, 5, 10, and 30 min TETA doping times. Since *R* shows the relative amount of $3\gamma$ annihilation from large pores or vacuum, we observe a large value of *R* at the surface and inner micrometer depth. In *R* plots of Figure 16, we observe an increase of *R* in the depth between 0.4 and 3 $\mu$m, which

**Table 3. Multilayer Analysis of *S* Data in PA Resin, PAN, and Modified PAN (m-PAN) Membranes[a]**

| | | | | diffusion length (nm) | | | density(g/cm$^3$) | | |
|---|---|---|---|---|---|---|---|---|---|
| sample | $S_1$ | $S_2$ | $S_3$ | $L_1$ (nm) | $L_2$ (nm) | $D_1$ | $D_2$ | $D_3$ | $\rho_1$ | $\rho_2$ | $\rho_3$ |
| m−PAN membr | 0.4804 ± 0.0006 | 0.4749 ± 0.0006 | 0.4783 ± 0.0008 | 200 ± 117 | 2788 ± 1576 | 61.7 ± 16.3 | 223 ± 165 | 2422 ± 86 | 1.2 ± 0.1 | 1.0 ± 0.1 | 0.7 ± 0.1 |
| PAN membr | 0.4795 ± 0.0005 | 0.4812 ± 0.0016 | 0.4731 ± 0.0020 | 978 ± 650 | 2076 ± 1392 | 51.5 ± 13.7 | 900 ± 502 | 4707 ± 1800 | 1.2 ± 0.2 | 1.0 ± 0.1 | 0.6 ± .1 |
| PA resin | 0.4613 ± 0.0004 | 0.4746 ± 0.0003 | | 43.6 ± 41.7 | | 3.76 ± 0.52 | 72 ± 38 | | 1.3 ± 0.1 | 1.3 ± 0.1 | |

[a] Notes: (1) PAN and m-PAN membranes are from three-layer fits and PA resin is from a two-layer fit. (2) $L_1$ and $L_2$ are the boundary lengths from fitted *S* parameters using VEPFIT.[75] (3) Diffusion lengths ($D_1$, $D_2$, $D_3$) are for Ps and positrons at the surface (skin), transition, and in the porous membranes, respectively. (4) $\rho_1$, $\rho_2$, and $\rho_3$ are the fitted densities for each layer.

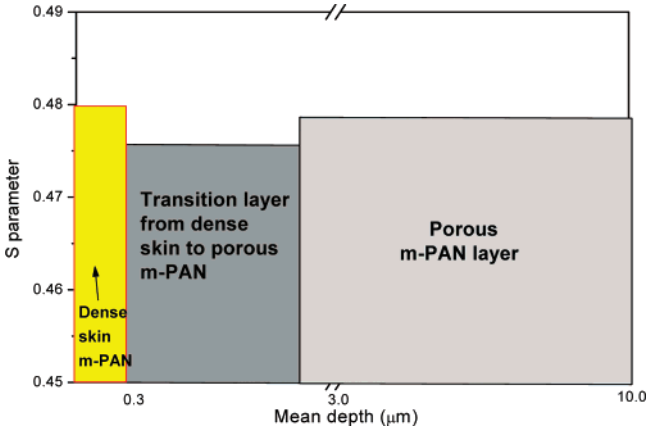


**Figure 13.** Schematic diagram of three layer depth structure obtained from VEPFIT analysis[75] of *S* parameter from DBES in the m-PAN membrane. The top layer is the dense skin of m-PAN, the second layer is a transition layer from dense skin to porous m-PAN, and the deep layer is the porous m-PAN.

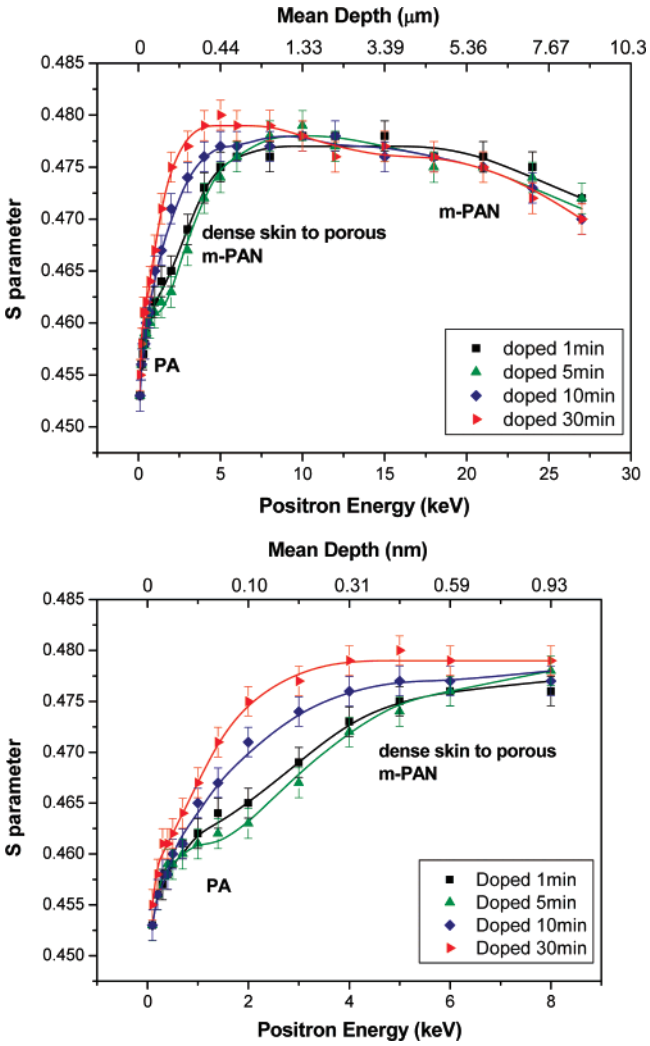


**Figure 14.** *S* parameters vs positron incident energy (or depth) in interfacial polymerized PA on m-PAN membrane at different times of TETA doping. The lines are from VEPFIT[75] fitted results in a three-layer model.

coincides with the locations of a large variation of *S* parameter vs depth plot as seen in Figure 14. The large pores inside a few micrometers with large pore sizes on the micrometer scale contribute to a further increase of *R* as the depth increases. The gradual increase of *R* with the increase of the depth indicates a

**Table 4. Multilayer Analysis of *S* Data and Pervaporation Performance in Interfacial Polymerized Polyamide/m-PAN Membranes**

| time of TETA doping (min) | $S_1$ | $S_2$ | $S_3$ | diffusion length (nm) $L_1$ (nm) | $L_2$ (nm) | density (g/cm$^3$) $D_1$ | $D_2$ | $D_3$ | $\rho_1$ | $\rho_2$ | $\rho_3$ | flux (g/m$^2$h) | water concn (wt %) |
|---|---|---|---|---|---|---|---|---|---|---|---|---|---|
| 30 | 0.4663 ± 0.0010 | 0.4801 ± 0.0005 | 0.4755 ± 0.0005 | 52 ± 14 | 734 ± 384 | 15 ± .3 | 51 ± 17 | 656 ± 700 | 0.9 ± 0.1 | 1.2 ± 0.1 | 0.9 ± 0.1 | 1306 ± 18 | 95.9 ± 0.1 |
| 10 | 0.4671 ± 0.0015 | 0.4791 ± 0.0007 | 0.4767 ± 0.0007 | 69 ± 23 | 627 ± 319 | 28 ± 7 | 124 ± 25 | 766 ± 694 | 0.9 ± 0.1 | 1.2 ± 0.1 | 0.9 ± 0.1 | 1094 ± 27 | 96.3 ± 0.7 |
| 5 | 0.4617 ± 0.0006 | 0.4795 ± 0.0005 | 0.4752 ± 0.0008 | 162 ± 49 | 2288 ± 623 | 19 ± 12 | 158 ± 48 | 900 ± 100 | 0.9 ± 0.1 | 1.2 ± 0.1 | 0.9 ± 0.1 | 1102 ± 24 | 98.6 ± 0.1 |
| 1 | 0.4649 ± 0.0007 | 0.4775 ± 0.0004 | 0.4761 ± 0.0013 | 274 ± 100 | 4210 ± 2355 | 28 ± 5 | 93 ± 34 | 2640 ± 1000 | 0.9 ± 0.1 | 1.2 ± 0.1 | 0.9 ± 0.1 | 1211 ± 34 | 98.4 ± 0.1 |

[a] Notes: (1) $L_1$ and $L_2$ are the boundary lengths from fitted *S* data using VEPFIT analysis.[75] (2) Diffusion lengths ($D_1$, $D_2$, $D_3$) are for Ps and positrons at the surface polyamide (PA), transition PA/m-PAN layer, and m-PAN/PAN of the membranes, respectively. (3) $\rho_1$, $\rho_2$, and $\rho_3$ are the fitted densities for each layer.

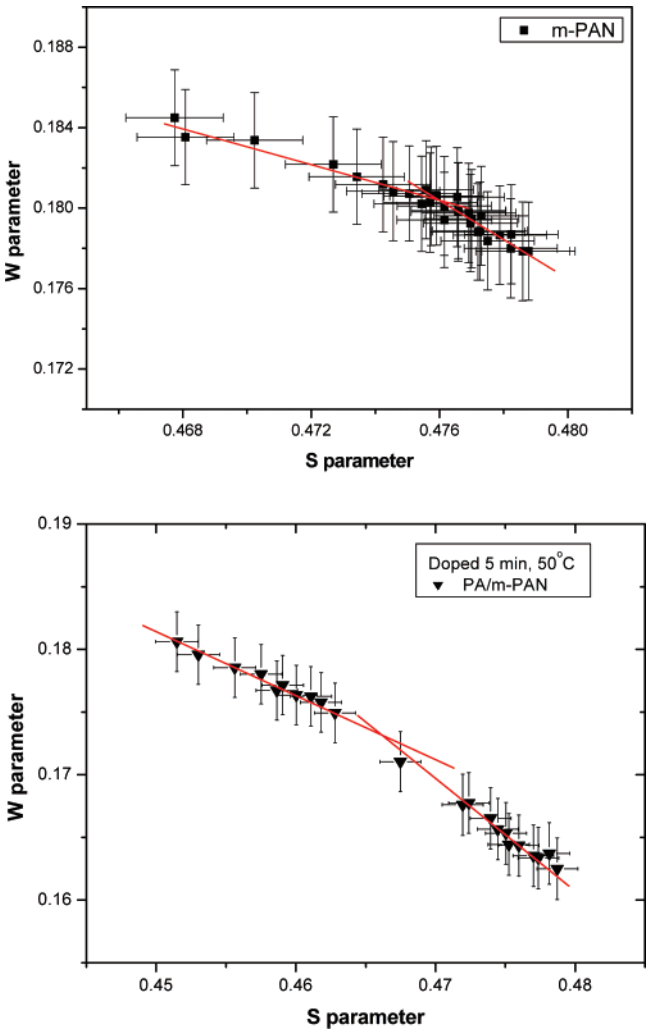


**Figure 15.** *S* vs *W* plot in the m-PAN membrane (top) and in interfacial polymerized PA/m-PAN membrane at 5 min TETA doping time (bottom). The lines were from two linear regressions fitting the data into two regions and the intercept indicates a significant transition from one layer to the other.

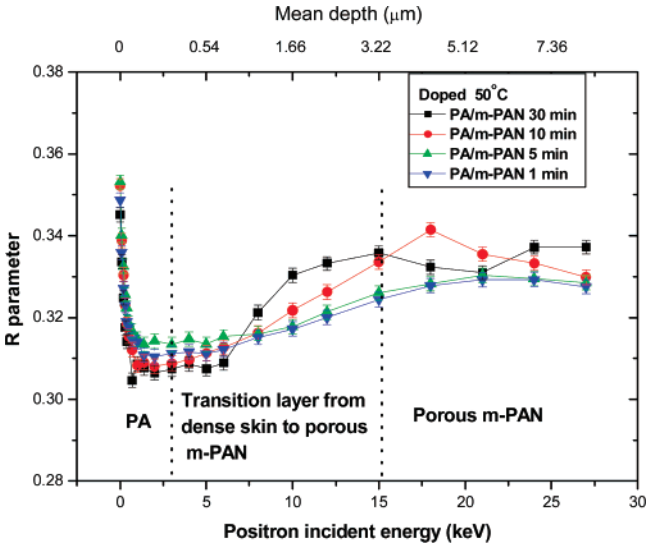


**Figure 16.** *R* parameters ($3\gamma/2\gamma$ annihilation ratio) vs positron incident energy (or depth) in interfacial polymerized PA on m-PAN membrane at different times of TETA doping. Vertical dot lines indicate the boundaries from layer to layer.

progressive transition from the dense layer to the porous m-PAN membrane as a function of depth in the region of micrometer

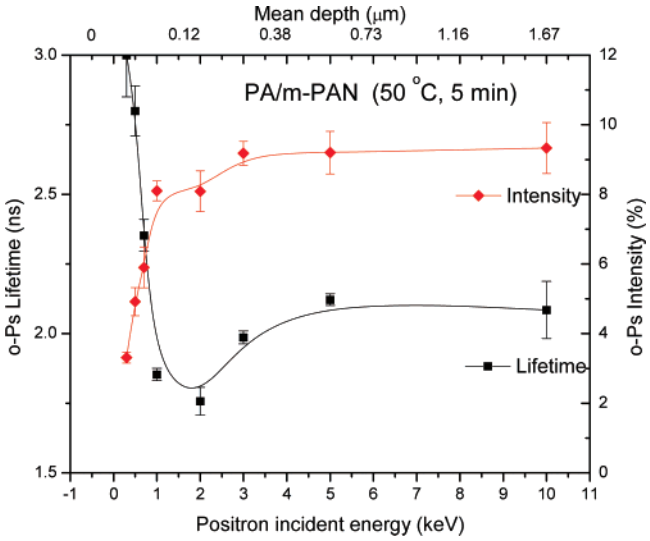


**Figure 17.** o-Ps annihilation lifetime ($\tau_3$) and intensity ($I_3$) vs positron incident emery (depth) in an interfacial polymerized PA on m-PAN membrane (5 min TETA doping time). Lines were drawn through data for eye-guide only.

depth. Although the trend of *R* variations with respect to the depth is similar for different TETA doping times and details are different. *R* data in Figure 16 provide evidence to support our assignments that the materials in layer 2 and layer 3 are m-PAN, where the amount of large pores progressively increases as a function of the depth.

To further identify the types of materials in each layer, we performed PAL experiments as a function of positron energy in one of interfacial polymerized PA membrane, i.e., 5 min TETA doping, which shows a clear kink (nearly flat region) of the first layer in *S* data (Figure 14). The analyzed $\tau_3$ and $I_3$ vs positron incident energy are shown in Figure 17. The raw PAL spectra are shown in Figure 6 as acquired at the AIST slow positron beam, where they have a better lifetime resolution and counting rates. It is worthwhile to mention that we have confirmed this set of PAL data using both the UMKC beam and also a newly built beam at Chung Yuan Christian University in Taiwan. As shown in Figure 17, we observe a sharp increase of $I_3$ near the surface which is a general phenomenon for the short diffusion length of o-Ps in polymeric materials. This feature is also seen in the *S* variation, which indicates p-Ps diffusion near the surface (Figure 14).

The values and variation of $\tau_3$ as a function of depth could be used to interpret the material types since PA and m-PAN have different o-Ps pick-off annihilation lifetimes as shown in Table 1. First we have observed a longer o-Ps lifetime near the surface due to o-Ps annihilation near the surface with a rough surface. In the depth between 1 and 3 keV, where we observed a kink (nearly flat region) of *S* vs depth in Figure 14, we also observe a dip of o-Ps lifetime ($\tau_3 = 1.76 \pm 0.04$ ns) in this region and then an increase of $\tau_3$ to a plateau of 2.1 ns. This is the trend that we would expect for a transition from PA to m-PAN because PA has a smaller free volume than m-PAN. It is noted that the observed lifetimes from beam experiments $\tau_3$ are not identical to the bulk lifetimes as presented in Table 1 because the slow positron beam is probing the membrane layers with a range of depth (depends on the positron energy) while the conventional PAL probes the average bulk lifetime. The positron energy distributions and dispersions of the measured depth are quite different between the beam and the conventional PAL experiments. The identification of the top layer as PA and the transition layer mainly as m-PAN is further supported by

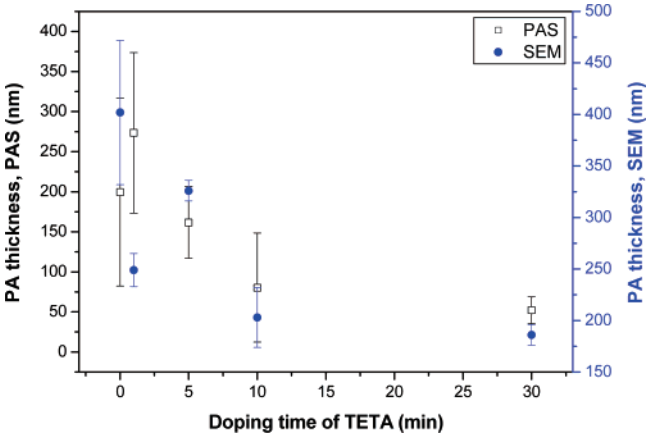


**Figure 18.** Skin layer thickness vs TETA doping time in PA on m-PAN membranes obtained from *S* parameter of positron annihilation (PAS) and from SEM images. The data for 0 min were the thickness for the dense skin m-PAN while the rest were for PA on m-PAN.

the observed o-Ps intensity ($I_3$) increases in Figure 17 from 8.0% to 9.33%, which is also consistent with the increase of o-Ps as shown for the bulk polymers from PA to m-PAN (Table 1). It is also noted that a kink in the $I_3$ plot of Figure 17 is similar to that in the *S* vs depth plots (Figure 14) because *S* is mainly contributed from p-Ps annihilation while $I_3$ is from o-Ps annihilation.

From the PAS data analyzed above, we have the assignments of layer materials as a function of depth from the surface as follows: PA (top layer), dense skin to porous m-PAN (transition layer), and porous m-PAN (third layer). We proceed to obtain the layer structure of interfacial polymerized PA membranes along with the AFM, and SEM data (Figures 9−11). From AFM images (Figure 9), we observed a smooth surface in m-PAN, and rough surfaces for interfacial polymerized PA membranes. The surface becomes less rough as a function of TETA doping time. Table 2 lists the measured surface roughness, $R_{ms}$ (mean square), $R_a$ (average), and $R_{max}$ (maximum) from AFM images from Figure 9. It is interesting that we observed that the trend of surface roughness with respect to TETA doping time is similar to the result of thickness of the skin layer in that both roughness and PA thickness decrease as a function of TETA doping time.

Next, we examine the cross section of the interfacial polymerized membranes by measuring SEM images as shown in Figures 10 and 11. We measured the top layer thickness as shown in Figures 10 and 11 and have three observations: (1) The skin layer, which is PA, is found to become thinner as a function of TETA doping time. (2) The apparent thickness of the second layer for the TETA-doped membranes is greater than the m-PAN membrane but there is a decreasing trend in the thickness of the transition layer as the TETA doping time increases.

The first observation is consistent with that of the observed top layer thickness from *S* parameter as a function of doping time. We plot this relationship relation between the skin thicknesses obtained by SEM and *S* parameter by the positron method and the TETA doping times as shown in Figure 18. It is interesting to observe a consistent result in the skin thickness obtained from two different methodologies although the absolute value of skin layer from SEM is seen to be slightly longer than that from PAS data. It should be noted that the skin thickness in SEM is a sum of formed skin PA l(as seen with surface roughness) and some swelled skin of m-PAN after TETA soaking effect, while in *S* data the skin is only due to PA which has a much lower value of *S* as a kink in the *S* vs depth plots (Figure 14).

It is interesting to observe a decrease of top layer PA thickness as a function of TETA doping time during the process of interfacial polymerization. It appears that as the time of TETA doping is longer, the amount of aqueous phase is getting deeper inside the dense layer of m-PAN and with more amount of TETA inside. The interfacial reaction (Figure 2) is a very fast reaction, and the product of polymerization, polyamide, will resist any further contact between TETA and TMC for further reaction. This is because PA has a small free volume (Table 1 and Figure 8) and the large reacting molecules such as TETA or TMC could not permeate through formed PA. In the case of longer doping TETA time, which has a higher concentration of TETA in the dense skin region of m-PAN, it will quickly form a thin impermeable layer of PA to resist further polymerization reaction. On the other hand, in the case of a short doping time, which has a less amount of TETA content in the m-PAN, will have less resistance to polymerization reaction and may allow to proceed further reaction and that would eventually lead to a thick PA layer on top of the dense m-PAN skin in the final membrane formation.

The second observation of an increase in the apparent second layer in TETA doped compared with the m-PAN membrane is also consistent with the *S*-parameter analysis that the skin m-PAN layer increases after TETA doping. For example, $L_1$, the top layer thickness in the m-PAN is only 200 ± 117 nm (Table 2) while the second boundary length (which includes $L_1$), $L_2$, varies from 734 to 4210 nm in interfacial polymerized PA membranes (Table 3). Due to the indistinguishable nature of the dense m-PAN skin and porous m-PAN in the transition layer from the VEPFIT analysis of *S* parameters in PA/m-PAN membranes, we should not take the resolved $L_2$ to quantitatively compare with the SEM images in this layer. One plausible explanation in the observed increase of the transition layer is due to the swelling effect of TETA soaking on the skin layer of m-PAN and the subsequent emersion of toluene in the polymerization processes. The TETA doping has apparently protected the original dense skin layer of m-PAN (ca. 400 nm) and the transition layer to be less reactive with TMC. The longer boundary length ($L_2$) in a shorter period time of TETA doping could be due to the similar resistant effect of the formation of the PA top layer.

On the basis of the PAS data (both DBES and PAL) and AFM, SEM data, we thus obtain the layer structure of PA/m-PAN membrane as: the top layer as PA, the second transition layer as dense to porous m-PAN, and the third layer as porous m-PAN. The obtained layer structure is schematically shown in Figure 19.

**III. Membrane Performance and Free-Volume Depth Parameters.** We have measured pervaporation performance of 70 wt % 2-propanol aqueous solution through the polyamide composite membranes, i.e., flux and water concentration in permeate. In Figure 20, we plotted the variation of flux and water concentration in permeate vs TETA doping time in the process of interfacial polymerization. It is seen that the flux is dramatically decreased by a factor of 4 with the presence of PA and the water concentration in permeate is also greatly improved from 46% to 95%. As shown in Figure 20 and Table 4 while the variation of TETA doping in PA polymerization could further improve the water concentration in permeate from 95.9% to 98.4% with different doping times while the flux has a reverse tend between 1102 and 1306 g/m$^2$h, which are still relative low in pervaporation applications. Since *S* data contains

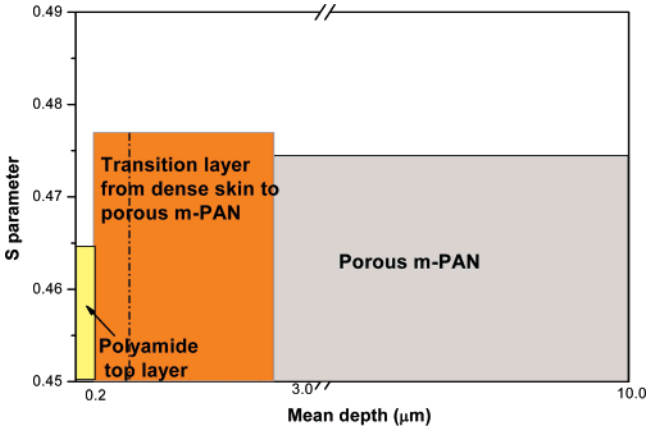


**Figure 19.** Schematic diagram of three-layer depth structure obtained from VEPFIT analysis[75] on *S* parameter of DBES data for PA on m-PAN membranes. The top layer is PA, and the second layer is a transition layer from dense to porous m-PAN, and the deep layer is the porous m-PAN membrane. The vertical dot line indicates the second layer includes sub-layers of the dense m-PAN and porous m-PAN in the three-layer VEPFIT analysis.

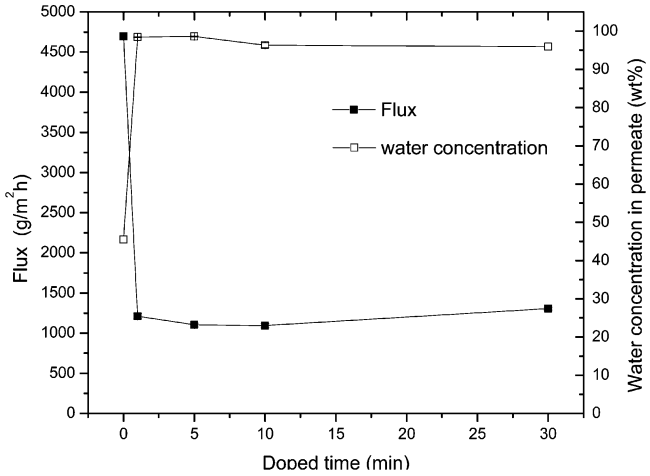


**Figure 20.** Flux and water concentration in permeate vs TETA doping time from pervaporation measurements in interfacial polymerized PA on m-PAN membrane systems. Lines connecting data points are for an eye guide only.

free volume information for polymeric systems, we proceed to examine the relationship between analyzed positron annihilation parameters in different layers and the membrane performance in pervaporation.

First, we plotted the top layer thickness ($L_1$) and the $S_1$ from the *S*-parameter analysis vs the flux and water concentration in permeate as shown in Figure 21. We found that the water concentration in permeate increases as a function of top layer PA thickness while the flux does not show a clear trend. The reasons of selectivity been controlled by the PA top layer are because PA has a free-volume size in between that of water and of 2-propanol (Figure 8) and also with a narrow free-volume size distribution. The current positron result is a good demonstration that PAL could provide a direct avenue to separate different types of molecules with different sizes and to select the desired molecules or to design the appropriate polymeric materials with the desired free-volume size distributions. The correlation between the PA thickness ($L_1$) and water concentration in permeate is shown as lines drawn through the data points in Figure 21 (top) in spite of the fact that PAS experiments were performed under vacuum while pervaporation measurements were performed under solvents. This direct relationship is due to the fact that the free-volume size distributions of both

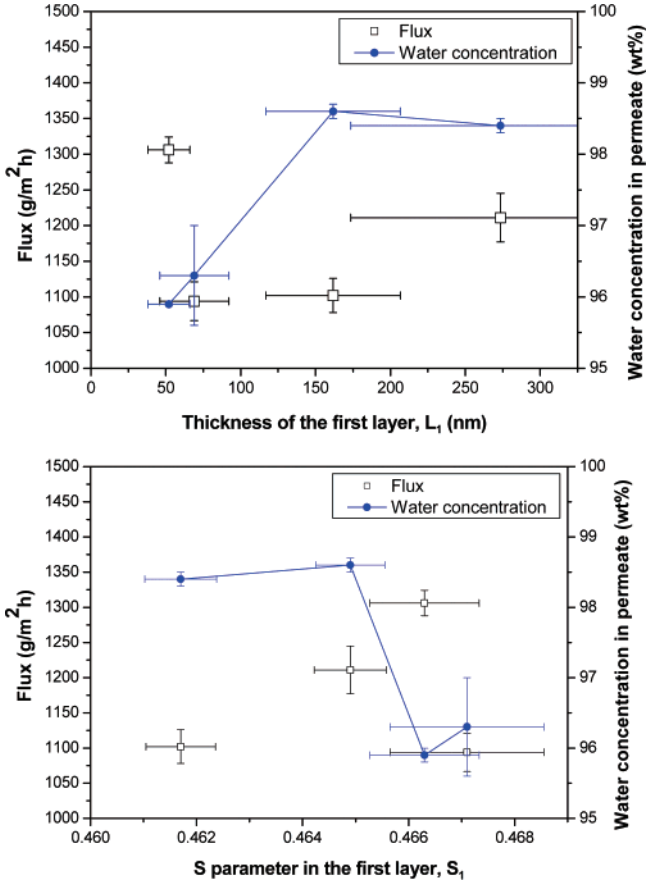


**Figure 21.** Flux and water concentration in permeate vs the top layer thickness $L_1$(top) and $S_1$ parameter (bottom) from positron experiments in interfacial polymerized PA on m-PAN membrane systems. Lines connecting data points are for an eye guide only.

wet and dry states PA are similar (Table 1 and Figure 8) yet still far apart from the kinetic diameters of water and 2-propanol (Table 1). The weak anticorrelations or no correlation between $S_1$ and water concentration in permeate (as shown in the connecting lines through the data points in the lower plot of Figure 21) are probably due to the resolving limit in the current VEPFIT analysis that the contribution of surface annihilation and back scattering of positrons and Ps to the top layer and also possibly a gap in physical properties between the nanoscopic (PAS) and macroscopic measurements (flux in pervaporation) in this membrane system.

Next, we examine the positron parameters of the second layer and any relationships with pervaporation performance. We plotted both second layer thickness, i.e., $L_2 - L_1$ and $S_2$ parameters vs flux and water concentration in the permeate in Figure 22. We observe a slight correlation between the second layer thickness and water concentration in permeate as shown in the connecting lines in the upper plot of Figure 22. Similar to $L_1$, a decrease of the second layer thickness as a function of TETA doping time may be also a result from the interfacial polymerized PA layer, since in VEPFIT analysis, the second layer includes the dense skin part of m-PAN. The lack of correlation between $L_1$, $S_1$, or $S_2$ and the flux and between $S_2$ and the water concentration in the permeate is probably due to the small variation of flux values at different doping times in this series of experiments and the limited experimental precisions in the current data. Further experiments with a large variation of flux and water concentration in the permeate by changing other experimental parameters, such as the TETA doping temperature or by changing chemical functional groups may

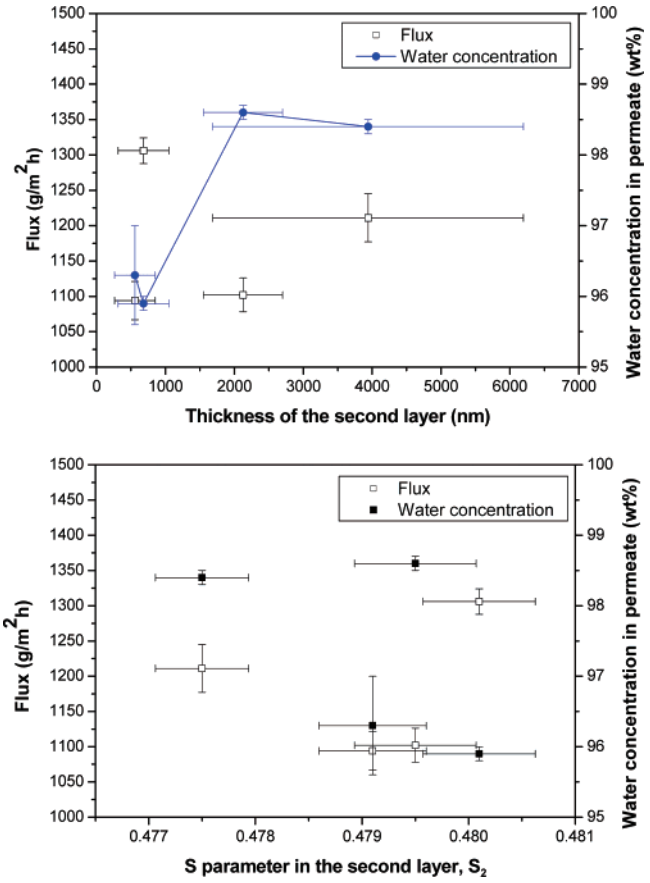


**Figure 22.** Flux and water concentration in permeate vs the second layer thickness (top) and $S_2$ parameter (bottom) from positron experiments in interfacial polymerized PA on m-PAN membrane systems. Lines connecting data points (top) are for an eye guide only.

be useful to address the relationship between flux (permittivity) and free-volume data in the future.

In summary, among data of flux, water concentration in permeate, and layer parameters from PAS data, we have observed a good correlation between the PA thickness and the water concentration in permeate, a slight correlation between the transition layer thickness and water concentration in permeate, weak anticorrelation or no correlation between fitted *S* parameters of each layer and water concentration in permeate, and no obvious correlations between the flux and positron parameters in this series of different TETA doping times of PA/m-PAN membrane systems.

## Conclusion

Positron annihilation spectroscopy coupled with a variable energy slow positron beam has been used to determine the layer structures and free-volume properties in an asymmetric polyamide membrane system prepared by interfacial polymerization. We found a three-layer structure in the m-PAN membranes, a dense skin (200−400 nm), a transitional layer from dense skin to porous m-PAN (0.3−3 $\mu$m) and a porous m-PAN layer. In interfacial polymerized PA membranes, we found a top PA layer on the order of 50−300 nm, and its thickness decreases with the TETA doping time. The thickness of this PA top layer plays a key role in the pervaporation performance, significantly increases water concentration in permeate for PA/m-PAN membrane systems. We also found that a progressive transition layer of PA/m-PAN layer (0.5−4 $\mu$m) exists, and it may play a secondary role in the pervaporation performance. These analyzed layer structures from PAS are compared with SEM and AFM images, which support the obtained results. Positron annihilation lifetime spectroscopy is a useful tool for quantitative analysis of free-volume size and distributions, which are important information to select the size of transporting molecules in pervaporation processes and to provide guidance for the design of multilayer thin-film polymers for membrane separation applications. It is our hope that combing PAS and the slow positron beam technique will provide an avenue to improve the membrane performance through a high degree of interaction, correlation, and comparison with physical, chemical, and engineering properties from conventional methods.

**Acknowledgment.** The authors wish to express their sincere gratitude to the National Science Council (NSC) and the Center-of-Excellence (COE) Program on Membrane Technology from the Ministry of Education (MOE), R.O.C., for the financial support.

## References and Notes

(1) Mulder, M. *Basic Principle of Membrane Technology*; Kluwer Academic Publisher: Dordrecht, The Netherlands, 1996.
(2) Hwang, S. T.; Kammermeyer, K. *Membrane in Separation*; John Wiley Sons: New York, 1975.
(3) Baker, R. W. *Membrane Technology and Application*; McGraw-Hill Companies: New York, 2000.
(4) Nunes, S. P.; Peinemann, K. V. *Membrane Technology in the Chemical Industry*; Wiley: Berlin, 2003.
(5) Wijmans, J. W.; Baker, R. W. *J. Membr. Sci.* **1995**, *107*, 1.
(6) Smitha, D.; Suhanya, D.; Scridhar, S.; Ramakrishna, S. *J. Membr. Sci.* **2004**, *241*, 1.
(7) Koros, W. J.; Coleman, M. R.; Walker, D. R. B. *Annu. Rev. Mater. Sci.* **1992**, *22*, 47.
(8) Gudernatsch, W.; Menzel, Th.; Strathmann, H. *J. Membr. Sci.* **1991**, *61*, 19.
(9) Shi, E.; Huang, W.; Xiao, Z.; Li, D.; Tang, M. *J. Appl. Polym. Sci.* **2007**, *104*, 2468.
(10) Li, C.-L.; Tu, C.-Y.; Inagaki, N.; Lee, K.-R.; Lai, J.-Y. *J. Appl. Polym. Sci.* **2006**, *102*, 909.
(11) Chen, H.; Liu, G.; Chakka, L.; Huang, S. H.; Lee, K. R.; Lai, J.-Y.; Sun, Y.-M.; Jean, Y. C. *Phys. Status Solidi C* **2007**, *4*, 3739.
(12) Niwa, M.; Kawanami, H. *Macromolecules* **2001**, *34*, 9039.
(13) Zhang, W.; Sato, T.; Smith, S. O. *Prog. Nucl. Magn. Reson. Spectrosc.* **2006**, *48*, 183.
(14) Dvinskikh, S. V.; Durr, U. H. N.; Yamamoto, K.; Ramamoorthy, A. *J. Am. Chem. Soc.* **2007**, *129*, 794.
(15) Khulbe, K. C.; Feng, C.; Matsuura, T.; Lamarche, G.; Lamarche, A. M. *Desalination* **2003**, *154*, 1.
(16) Lou, Y.; Ge, M.; Freed, J. H. *J. Phys. Chem. B* **2001**, *105*, 11053.
(17) Lin, K.-Y.; Wang, D.-M.; Lai, J.-Y. *Macromolecules* **2002**, *35*, 6697.
(18) Cha, B. J.; Kang, Y. S.; Won, J. *Macromolecules* **2001**, *34*, 6631.
(19) Hamad, F.; Khulbe, K. C.; Matsuura, T. *J. Membr. Sci.* **2005**, *256*, 29.
(20) McKee, C. T.; Mosse, W. K. J.; Ducker, W. A. *Rev. Sci. Instrum.* **2006**, *77*, 053706.
(21) Brant, J. A.; Childress, A. E. *Environ. Eng. Sci.* **2002**, *19*, 413.
(22) Doucet, F. J.; Maguire, L.; Lead, J. R. *Anal. Chim. Acta* **2004**, *522*, 59.
(23) Xiang, H.; Shin, K.; Kim, T.; Moon, S. I.; McCarthy, T. J.; Russell, T. P. *Macromolecules* **2005**, *38*, 1055.
(24) Pujari, P. K.; Sen, D.; Amarendra, G.; Abhaya, S.; Pandey, A. K.; Dutta, D.; Mazumder, S. *Nucl. Instrum. Methods Phys. Res., Sect. B* **2007**, *254*, 278.
(25) Torok, G.; Lebedev, V. T.; Cser, L.; Buyanov, A. L.; Revelskaya, L. G. *Mater. Sci. Forum* **2000**, *321*, 470.
(26) McQuaw, C. M.; Sostarecz, A. G.; Zheng, L.; Ewing, A. G.; Winograd, N. *Appl. Surf. Sci.* **2006**, *252*, 6716.
(27) Ahmad, A. L.; Mohd. Nawawi, M. G.; So, L. K. *Sep. Sci. Technol.* **2005**, *40*, 3071.
(28) Cohen, M. H.; Turnbull, D. *J. Chem. Phys.* **1959**, *31*, 1164.
(29) Park, J. Y.; Paul, D. R. *J. Membr. Sci.* **1997**, *125*, 1.
(30) For example, see: *Principles and Applications of Positron and Positronium Chemistry*; Jean, Y. C., Mallon, P. E., Schrader, D. M., Eds.; World Sci.: Singapore, 2003.
(31) For example, see: *Positron Spectroscopy of Solids*; Dupasquier, A., Mills, A. P., Jr., Eds.; ISO Press, Amsterdam, 1993.
(32) For example, see: Jean, Y. C. *Microchem. J.* **1990**, *42*, 72.

(33) Consolati, G.; Pegoraro, M.; Quasso, F.; Severini, F. *Polymer* **2001**, *42*, 1265.
(34) Hill, A. J.; Bastow, T. J.; Meakin, P.; Turney, T. W.; Hoang, M.; Scalera, N.; Pertici, P.; Vitulli, G. *Desalination* **2002**, *144*, 61.
(35) Dlubek, G.; Redmann, F.; Krause-Rehberg, R. *J. Appl. Polym. Sci.* **2002**, *84*, 244.
(36) Nagel, C.; Gunther-Schade, K.; Fritsch, D.; Strunskus, T.; Faupel, F. *Macromolecules* **2002**, *35*, 2071.
(37) Dutta, D.; Bhattacharyya, A.; Ganguly, B. N. *J. Membr. Sci.* **2003**, *224*, 127.
(38) Sharma, A.; Thampi, S. P.; Suggala, S. V.; Bhattacharya, P. K. *Langmuir* **2004**, 4708.
(39) Garcia, A.; Iriarte, M.; Uriarte, C.; Iruin, J. J.; Etxeberria, A.; Del, Rio, J. *Polymer* **2004**, *45*, 2949.
(40) Satyanarayana, S. V.; Bhattacharya, P. K. *J. Membr. Sci.* **2004**, *238*, 103.
(41) Winberg, P.; Eldrup, M.; Pedersen, N. J.; Van Es, M. A.; Maurer, F. H. J. *Polymer* **2005**, *46*, 8239.
(42) Kruse, J.; Kanzow, J.; Ratzke, K.; Faupel, F.; Heuchel, M.; Frahn, J.; Hofmann, D. *Macromolecules* **2005**, *38*, 9638.
(43) Satyanarayana, S. V.; Subrahmanyam, V. S.; Verma, H. C.; Sharma, A.; Bhattacharya, P. K. *Polymer* **2006**, *47*, 1300.
(44) Wang, X.-Y.; Willmore, F. T.; Raharjo, R. D.; Wang, X.; Freeman, B. D.; Hill, A. J.; Sanchez, I. C. *J. Phys. Chem. B* **2006**, *110*, 16685.
(45) Fang, Z.; Xu, Y.; Tong, L. *J. Apply. Polym. Sci.* **2006**, *102*, 2463.
(46) Yampolskii, Y.; Shantarovich, V. In *Materials Science of Membranes for Gas and Vapor Separation*; Yampolskii, Y., Pinnau, I., Freeman, B. D., Eds.; Wiley Intersci. Pub.: New York, 2006; pp 191−210.
(47) Schultz, P. J.; Lynn, K.G. *Rev. Mod. Phys.* **1998**, *60*, 701.
(48) *Positron Beams and Their Applications*; Coleman, P., Ed.; World Sci. Pub.: Singapore, 2000.
(49) Huang, S.-H.; Li, C.-L.; Hu, C.-C.; Tsai, H. A.; Lee, K. R.; Lai, J. Y. *Desalination* **2006**, *200*, 387.
(50) Zhang, R.; Cao, H.; Chen, H. M.; Mallon, P.; Sandreczki, T. C.; Richardson, J. R.; Jean, Y. C.; Nielsen, B.; Suzuki, R.; Ohdaira, T. *Radiat. Phys. Chem.* **2000**, *58*, 639.
(51) Chen, H.; Zhang, R.; Li, Y.; Zhang, J.; Wu, Y. C.; R.; Sandreczki, T. C.; Mallon, P. E.; Suzuki, R.; Ohdaira, T.; Gu, X.; Nguyen, T.; Jean, Y. C. *Mater. Sci. Forum* **2004**, *445*−*46*, 274.
(52) Kobayashi, Y.; Kojima, I.; Hishita, S.; Suzuki, T.; Asari, E.; Kitajima, M. *Phys. Rev. B* **1995**, *52*, 823.
(53) Jean, Y. C.; Zhang, R.; Cao, H.; Yuan, J.-P.; Huang, C.-M.; Nielsen, B.; Asoka-Kumar, P. *Phys. Rev. B* **1997**, *56*, R8459.
(54) Li, Y.; Zhang, R.; Chen, H.; Zhang, J.; Suzuki, R.; Ohdaira, T.; Feldstein, M. M.; Jean, Y. C. *Biomacromolecules* **2003**, *4*, 1856.
(55) Suzuki, R.; Ohdaira, T. Mikado, T.; Uedono, A.; Ohgaki, T.; Yamazaki, T.; Tanigawa, S. *Mater. Sci. Forum* **1997**, *255*, 114.
(56) PATFIT package (1989) purchased from Riso National Laboratory, Riso, Denmark.
(57) Cao, H.; Dai, G. H.; Yuan, J.-P.; Jean, Y. C. *Mater. Sci. Forum* **1997**, *238*, 255.
(58) Kansy, J. *Nucl. Instrum. Methods Phys. Res., Sect. A* **1996**, *374*, 235.
(59) Shukla, A.; Peter, M.; Hoffman, L. *Nucl. Instrum. Methods Phys. Res., Sect. A* **1993**, *335*, 310.
(60) Jean, Y. C. *Macromolecules* **1996**, *27*, 5756.
(61) DeMaggio, G. B.; Frieze, W. E.; Gidley, D. W.; Zhu, M.; Hristov, H.; Yee, A. F. *Phys. Rev. Lett.* **1997**, *78*, 1624.
(62) Cao, H.; Zhang, R.; Zhang, J.-P.; Huang, C.-M.; Jean, Y. C.; Suzuki, R.; Ohdaira, T.; Nielsen, B. *J. Phys.: Condens. Matter* **1998**, *10*, 10429.
(63) Algers, J.; Suzuki, R.; Ohdaira, T.; Maurer, F. H. J. *Polymer* **2004**, *45*, 4533.
(64) Jean, Y. C; Zhang, J.; Chen, H.; Li, Y.; Liu, G. *Spectrochim. Acta, Part A* **2005**, *61*, 1683.
(65) Tao, S. J. *J. Chem. Phys.* **1972**, *56*, 5499.
(66) Eldrup, M.; Lightbody, D.; Sherwood, J. N. *Chem. Phys.* **1981**, *63*, 51.
(67) Nakanishi, N.; Wang, S. J.; Jean, Y. C. In *Positron Annihilation Studies of Fluids*; Sharma, S. C., Ed.; World Scientific: Singapore 1988; p 292.
(68) Shimazu, A.; Ikeda, K.; Miyaki, T.; Ito, Y. *Radiat. Phys. Chem.* **2000**, *58*, 551.
(69) Kim, S. H.; Kwak, S.-Y.; Suzuki, T. *Environ. Sci. Technol.* **2005**, *39*, 1764.
(70) Debowska, M.; Piglowski, J.; Slusarczyk, C.; Rudzinska-Girulska, J.; Suzuki, T.; Yu, R. *Radiat. Phys. Chem.* **2007**, *76*, 325.
(71) Breck, D. W. *Zeolite Molecular Sieve Structure, Chemistry and Use*; Wiley, New York, 1974; pp 30−42.
(72) Van der Bruggen, B.; Schaep, J.; Wilms, C.; Vandecasteele, *J. Membr. Sci.* **1999**, *156*, 29.
(73) Teng, M.-Y.; Lee, K.R.; Liao, D.-J.; Lin, Y.-S.; Lai, J.-Y. *Eur. Polym. J.* **2000**, *26*, 663.
(74) Hirata, K.; Kobayashi, Y.: Ujihira, Y. *J. Chem. Soc., Faraday Trans.* **1996**, *92*, 985.
(75) Van Veen, A.; Schut, H. H.; de Vries, J.; Hakvoort, H. A.; IJpma, M. R. *AIP Conf. Proc.* **1990**, *218*, 171.

MA071493W